# New archeomagnetic directional records from Iron-Age southern Africa (ca. 425–1550 CE) and implications for the South Atlantic Anomaly

Vincent J. Hare<sup>1</sup>, John A. Tarduno<sup>1,2,3</sup>, Thomas Huffman<sup>4</sup>, Michael Watkeys<sup>3</sup>, Phenyo C.

Thebe<sup>5</sup>, Munyaradzi Manyanga<sup>6</sup>, Richard K. Bono<sup>1</sup>, Rory D. Cottrell<sup>1</sup>

<sup>1</sup>Department of Earth and Environmental Sciences, University of Rochester, Rochester, New York 14627, USA
 <sup>2</sup>Department of Physics and Astronomy, University of Rochester, Rochester, New York 14627, USA

<sup>3</sup>School of Geological Sciences, University of KwaZulu-Natal, Durban 4000, South Africa

<sup>4</sup>School of Geography, Archaeology and Environmental Studies, University of the Witwatersrand, Johannesburg 2050,

South Africa

<sup>5</sup>Archaeology Unit, Department of History, University of Botswana, Gaborone 0022, Botswana

<sup>6</sup>History Department, University of Zimbabwe, Harare, Zimbabwe

# **Key Points:**

- New archaeomagnetic directions from the Iron Age (425-1550 CE) of southern Africa
- · Directional changes suggest recurrent flux-expulsion at the core-mantle boundary
- Relationship with archaeomagnetic jerks and a long-lived South Atlantic Anomaly is identified

Corresponding author: Rory D. Cottrell, rory.cottrell@rochester.edu

#### Abstract

19

20

22

28

29

30

32

41

43

50

The paucity of Southern Hemisphere archaeomagnetic data limits the resolution of pale-osecular variation models. At the same time, important changes in the modern and historical field, including the recent dipole decay, appear to originate in this region. Here, a new directional record from southern Africa is presented from analysis of Iron Age (ca. 425-1550 CE) archaeological materials, which extends the regional secular variation curve back to the first millennium. Previous studies have identified a period of rapid directional change between 1225 and  $\sim$ 1550 CE. The new data allow us to identify an earlier period of relatively rapid change between the  $6^{th}$  and  $7^{th}$  centuries CE. Implications for models of recurrent flux-expulsion at the core-mantle boundary are discussed. In addition, we identify a possible relationship of changes recorded in these African data with archaeomagnetic jerks.

#### 1 Introduction

The rapid decay of Earth's dipole moment over the past two centuries [Gubbins et al., 2006; Jackson et al., 2000] is also associated with rapid changes in field morphology [Hulot et al., 2002]. These observations have prompted speculation that the present behavior of the geodynamo is unusual [De Santis and Qamili, 2008; Laj and Kissel, 2015; Pavón-Carrasco and De Santis, 2016], and provide motivation for improving our knowledge of the temporal evolution of the geodynamo further back in time. In particular, efforts have focussed on improving the spatial and temporal coverage of archeo- and paleomagnetic records over the past two millennia. However, such data are overwhelmingly (>90%) biased towards the Northern Hemisphere, which limits the resolution of paleosecular variation (PSV) models. Additionally, the present decay in dipole moment appears to be strongly associated with both the growth of reversed flux patches at the core-mantle boundary (CMB) in the Southern Hemisphere, as well as the expansion and deepening of the surface intensity low which defines the South Atlantic Anomaly (SAA) - an important feature of the ionosphere. Longer-term data from this region are crucial to understanding the current trend.

Although several recent studies have improved coverage over the African continent, e.g. archeointensities [*Mitra et al.*, 2013; *Kapper et al.*, 2017] and directions [*Donadini*, 2015] from west African archaeological sites, these locations remain at least 40 degrees north of the CMB reversed flux patch (i.e. extrapolated to a surface location) linked to

the present-day SAA. We recently presented the first archeomagnetic data from Iron Age 51 sites of southern Africa (~1000-1550 CE) [Neukirch et al., 2012; Tarduno et al., 2015]. 52 These records show a sharp intensity drop (0.054  $\mu$ T/yr) after ca. 1270 CE, at a rate comparable to modern field changes in the SAA, but to lower values. This was accompanied by rapid directional change of between 0.1 °/yr to 0.12 °/yr during the period 1225 to ~1550 CE. The pattern of changes motivated the model proposed by [Tarduno et al., 2015] whereby the recurrence of low field values reflects magnetic flux expulsion from the core, promoted by the unusual CMB composition and structure beneath southern Africa as defined by seismology [Lekic et al., 2012; Cottaar and Lekic, 2016]. There are virtually no archaeomagnetic data from southern Africa before ca. 1000 CE, which are needed to 60 test the model of recurring flux expulsion episodes. We have therefore shifted focus to Botswana and Zimbabwe to sample early Iron Age structures that would extend the direc-62 tional sequence back to the first millennium CE. 63

#### 2 Archaeological collection

73

79

82

We have identified and sampled the remains of burnt daga (mud) grain bins, hut floors and cattle enclosures (*kraals*) from well-dated Early and Late Iron Age localities around the Shashe-Limpopo confluence and surrounding plateaus (see Figure 1) in northern South Africa, Botswana and Zimbabwe. Most grain bins, hut floors and kraals are now found as isolated patches amid brush vegetation common in southern Africa. Further archeological context can be found in *Huffman* [2007] (see also supporting information [*Huffman*, 1978; *Huffman and du Piesanie*, 2011; *Huffman et al.*, 2013, 2016; *Huffman and Woodborne*, 2016; *Main*, 2002, 2008; *Robinson*, 1961]. These localities fill gaps in previous records, and extend the directional curve back to the 4<sup>th</sup> century. The material, previously unstudied, is similar to that already reported in *Neukirch et al.* [2012] and *Tarduno et al.* [2015], and dated to various episodes in the first millenium CE, with the exception of one locality (Faure Ruins, FR) which dates to the 16<sup>th</sup> century. All localities are dated by AMS radiocarbon analysis of associated organic material, and/or the stylistic sequence of pottery [*Huffman*, 2007] associated with the archaeological assemblage.

The Iron Age in southern Africa began with several phases of migration of Bantuspeaking peoples from central and west Africa. They cultivated various grains, developed complex metal-working technologies, and lived in villages which included grain bins, huts and cattle enclosures [*Huffman*, 2007]. It has been established that ritualistic burning of daga structures [*Huffman*, 2009a] was performed in response to periods of prolonged drought [*Huffman and Woodborne*, 2016].

We collected fragments from 4 grain bin localities (Rhino Mine I, "RMEI"; Rhino Mine II, "RMEII"; Mabveni, "MB"; Buhwa, "SL"), one hut floor locality (Manong East, "ME"), and one kraal locality (Faure Ruins, "FR"), all of which appear to have been ritualistically burnt (supporting information, Figure S1). Burnt fragments were collected from in situ material during 2014 and 2016 field seasons, and orientated with Sun and Brunton compasses. In appearance, the grain bin materials consisted of a mixture of fine grained red clays with millimeter-sized quartz pebble inclusions, which experienced high temperatures and rapid cooling. The kraal materials were originally a mixture of cattle dung, grass, clay and wood, which formed a grey-green vesicle-rich glass with a mixture of black glass upon heating to high temperatures. The RME grain bins were exposed by iron ore mining operations in the vicinity, but apparently not disturbed from their original positions. Because the area is rich in iron ore, we conducted a field survey (see supporting information) to map possible magnetic anomalies using a Grad601 high-resolution fluxgate gradiometer (Bartington Instruments). The observed field anomaly around the localities was sufficiently low (< 200 nT) to ensure that grain bin materials acquired a directional signal representative of the geomagnetic field during cooling after firing (supporting information, Figure S4).

# 3 Magnetic mineralogy

83

86

93

100

101

102

103

105

107

109

110

111

112

113

114

Rock magnetic experiments were performed at the University of Rochester to characterize magnetic mineralogy. Low-field susceptibility versus temperature measurements were performed on bulk powdered material in air using an KLY4-CS Kappabridge (AGICO). The results indicate stability upon heating, with Curie temperatures in the 560 to 600 °C range. Magnetic hysteresis and first order reversal curves (FORCs) [*Pike et al.*, 1999] were measured using an alternating gradient force magnetometer (MicroMag 2900, Princeton Measurements Corporation). These indicate the presence of non-interacting SD/PSD grains, consistent with magnetite/titanomagnetite carriers (see Figure 2, Figure S2-S3 [*Day et al.*, 1977; *Dunlop*, 2002]), with some high coercivity background phase in most samples, likely pigmentary hematite. For one locality, ME, hysteresis loops are slightly wasp-waisted, which suggests the presence of two remanence-carrying fractions of different coercivities. Magnetic susceptibility data indicate the dominance of a magnetite or

near-magnetite carrier. Various degrees of reproducibility were observed in cooling curves, indicative of changes in domain state or composition. The latter suggest the presence of minor magnetic phases (e.g., maghemite, hematite).

#### 4 Archaeomagnetic directions

Cube specimens (~ 1 cm³) were prepared for laboratory measurements using a bronze rock saw (UK-650, ASC Scientific), which was kept cool by the application of a moist sponge to the blade during operation (Figure S1). After cutting and drying, specimens were stored for several days in the magnetically-shielded room (ambient field < 200 nT) at the University of Rochester. Measurements were then performed with a 755R DC-SQUID magnetometer (2G Enterprises) with high resolution sensing coils. Alternating field (AF) demagnetizations were conducted in 5 mT steps from 5 mT to 40 mT, and thereafter in 10 mT steps to 100 mT using a SI-4 AF demagnetizer (Sapphire Instruments). Thermal demagnetizations were also performed on specimens from each fragment in 25 °C steps from 150 °C to 625 °C using a TD48-SC thermal demagnetizing oven (ASC Scientific).

Orthogonal vector plots display stable single-component magnetizations which trend to the origin during both AF and thermal treatments (Figure 3(a-f). For most specimens, approximately 50-70 % of NRM is lost between the 10 and 50 mT demagnetization steps. After the 100mT AF treatment, ~20 % of the original NRM is retained, suggesting the presence of a high-coercivity hematite phase. Directions obtained by principal component analysis [Kirschvink, 1980] in a range between 15 mT and 100 mT (depending on specimen) display maximum angle of deviation (MAD) values generally less than 3°. Specimen directions were then used to calculate the Fisher mean directions and 95% confidence interval [Fisher, 1953]. Prior thermal remanent magnetization (TRM) acquisition experiments show no evidence for TRM anisotropy [Tarduno et al., 2015] in these materials.

Most of our samples showed acceptable MAD values (more than half of MAD values are less than 2.3°), but occasionally MAD values are much greater (5-21°). These MAD values, as well as dispersions associated with some mean directions, are higher than seen in studies of archeomagnetic materials obtained elsewhere (e.g. Europe) and most likely reflect the heterogeneous nature of the material, and post-firing disturbance and alteration (weathering). Accordingly, we adopted a stringent procedure to identify and exclude outliers. The procedure is similar to that used by *Tema and Kondopoulou* [2011] and

Pavón-Carrasco et al. [2010]. Briefly, we reject outlier directions which display angular distances more than  $3\times\alpha_{95}$  from the Fisher mean direction of each locality. The mean and  $\alpha_{95}$  is then recomputed without the outlier direction(s). Using this procedure we excluded between 0 (RME2) and 6 (ME) specimens per locality. More information about this procedure can be found in supporting information (Figure S6), and all individual specimen data may be accessed on the MagIC database. Because we believe each burnt structure at a locality is of the same age, each fragment has approximately the same number of measured samples at a locality, and there is scatter at the specimen level (detected by our outlier analysis, see tables S2-S7), specimen directions were grouped at the locality level (Table 1). An exception to this is the splitting of RME into two occupation ages (Table 1, supporting information). Values of  $\alpha_{95}$  were generally around  $\sim 5^{o}$  (see Table S1), and only one site, FR, exhibited an  $\alpha_{95}$  value greater than  $5^{o}$ .

146

147

149

151

152

153

154

155

156

157

158

160

162

163

164

165

166

167

169

171

172

173

174

175

176

177

178

Finally, we reduced locality mean directions to the location of Mapungubwe (22.212  $^o\mathrm{S},\,29.387$   $^o\mathrm{E}),$  the capital of a pre-colonial Iron Age Kingdom. Mapungubwe is an important archaeological site geographically located at the approximate center of our site distribution, making it a convenient choice for the reduction. Mean directions were reduced to these coordinates using virtual geomagnetic poles, VGPs [Shuey et al., 1971]. The magnitude of the correction is between 0.1 and  $5^{\circ}$ . To estimate the error due to VGP reduction we compared the International Geomagnetic Reference Field (IGRF) value for each locality for the year 2010, reduced to the location of Mapungubwe, with the known value (Dec,  $346.98^{\circ}$ ; Inc,  $-60.56^{\circ}$ ). The angular difference between directions is less than 2°, which is similar to the result obtained for archaeomagnetic data from western Europe [Gallet et al., 2002] using an identical procedure. However, we caution that gradients may have been greater (and greater than in Europe) in the past and the VGP reduction procedure we have employed should only be taken as a guide. The progression of unreduced directions is shown in Figure S5. Table 1 shows the final site mean directions and statistics. A complete list of individual specimen directions may be found in the supporting information.

In Figure 4 we plot our records on an equal-area stereonet, combined with earlier data from *Neukirch et al.* [2012] and *Tarduno et al.* [2015]. The new results define a coherent loop in the archeomagnetic curve for southern Africa between ca. 425 and ca. 1370 CE. In other words, the earliest site (SL, 400-450 CE) shows directions which are statistically indistinguishable from those more than 900 years later (AD 160, 1317-1415 CE).

Here we divide this new archeomagnetic directional path into 5 arc segments, separated by cusps (Figure 4, SI Table S8). While this division is somewhat subjective, we feel our choice accurately reflects the important trends defined by the data. Other divisions, that are sensitive to the need to average over intervals long enough such that uncertainties in age and direction do not obscure the major trends (>100 yr) yield similar rates. Previous work identified a period of relatively rapid directional change between 1225 and ca. 1550 CE (>0.1 °/yr). In our new data, we see an earlier period of relatively rapid change between ca. 400–450 and ca. 550–570 CE, and again between 550–570 CE and 750–800 CE, during which the rate of change was approximately 0.1 °/yr. This is more rapid than the modern rate of change in the Limpopo region of 0.07 °/yr (here estimated from the IGRF direction and the predicted direction for 1840 from the CALS3k.4 [*Korte et al.*, 2009] model).

## 5 Discussion

Rapid directional changes between 1225 and  $\sim$  1550 CE are accompanied by intensity values which are lower than the present-day regional low, which is associated with Southern Hemisphere reversed flux patches at the CMB [Tarduno et al., 2015; Terra–Nova et al., 2017]. This is suggestive of repeated episodes of flux expulsion associated with the African Large Low Shear Velocity Province (LLSVP) influencing core flow (driving the magnetic Reynolds number toward unity) leading to reversed flux [Tarduno et al., 2015]. The longevity of the LLSVP suggests that flux expulsion could be a recurring feature in this region. Therefore, similar episodes of rapid directional change are expected further back in time. Whilst not as rapid as the changes in the  $15^{th}$  century, the directional variations identified between 400–450 CE and 750-800 CE may indicate a similar flux expulsion episode. However, archaeointensity values from this period are needed for further clarity.

It is interesting to compare our Iron Age directional records with PSV models (Figure 5(a-e)). There is disagreement between our data and the predictions of CALS3k.4 [Korte and Constable, 2011], particularly in inclination in the 1st Millennium CE, whereas model PFM9k [Nilsson et al., 2014] does not represent the directional loop seen in the data (see also supporting information, Figure S7). In contrast, some other models weighted toward archeomagnetic data predict a directional loop similar to that seen in the data, but at somewhat different times and predicted declinations (ARCH3k.1(MAST), Korte et al.

[2009], A\_FM, *Licht et al.* [2013] and SHA\_DIF\_14K, *Pavón-Carrasco et al.* [2014]). The general agreement of data and predictions from A\_FM, ARCH3k.1(MAST) and SHA\_DIF\_14K is surprising; these models are strongly biased toward North Hemisphere data and their accuracy for South Hemisphere locations is expected to be limited.

Gallet et al. [2003] originally identified phenomena known as "archaeomagnetic jerks" in secular variation records from western Europe, showing repeated periods of sharp directional variation which coincide with strong hemispheric field asymmetry, defined in terms the maximum ratio of the quadrupolar to the dipolar energies at the Earth's surface,  $\langle Q \rangle / \langle D \rangle$ . Gallet et al. [2009] found a correlation between the regional signature of these episodes and periods of strong relative quadrupole moment at ~200 CE, ~800 CE and ~1400 CE which led them to believe that the mechanism behind archaeomagnetic jerks was of global origin. They suggest that these features were caused by transient hemispherical asymmetry of flux patches at the CMB, which Dumberry and Finlay [2007] speculated were due to a long term influence of the lowermost mantle on thermal coupling.

In Figure 5(f) we show the ratio of quadrupole  $\langle Q \rangle$  to dipole  $\langle D \rangle$  energies for three models [i.e., ARCH3k.1(MAST), A\_FM and SHA\_DIF\_14K], that best approximate the archeomagnetic loop seen in our new data, together with the times of the archeomagnetic jerks identified by *Gallet et al.* [2009]. *Pavón-Carrasco et al.* [2014] also discuss quadrupole/dipole energies versus time. There is excellent agreement between the rapid changes in the southern African data between ca. 1225 and ca. 1550 CE and the archeomagnetic jerk proposed by *Gallet et al.* [2009] at ca. 1400 CE. The rapid changes are also very clear in the ARCH3k.1(MAST) and SHA\_DIF\_14K models, but not well expressed in the A\_FM model.

Rapid changes in the southern African data, and the ARCH3k.1(MAST), A\_FM and SHA\_DIF\_14K models occur close to the archeomagnetic jerk proposed at ca. 800 CE. However, the southern African record appears to be offset slightly (100 yr or less) from the proposed archeomagnetic jerk. The offset might reflect limited resolution of our data near 800 CE, or inaccuracies in PSV models.

Irrespective of differences in between the models and data uncertainties, the approximate agreement between the times of rapid changes reflected in PSV models weighted toward archeomagnetic data, and our new records appears to corroborate the interpretation [Gallet et al., 2009] that global features are present in the European data. The consistency

of regional data from such different contexts adds weight to the suggestion that the underlying mechanism must be of global origin. We speculate that the phenomenon of archeomagnetic jerks is consistent with repeated flux expulsion at the CMB, ultimately caused by core flow influenced the African LLSVP.

We note that the episode at ca. 1400 CE appears to be a particularly robust feature, and is also reported in sedimentary directions from the coastal lake of Eilandvlei, on the south coast of South Africa [Wündsch et al., 2016]. Directional measurements of volcanic sequences from Marion Island [Amerigian et al., 1974], southeast of South Africa, show that the present high rates of directional change persisted during the past 500 kyr, further supporting the suggestion that repeated flux expulsion, and the SAA, are long-term features of the field.

## 6 Conclusion

To understand present-day and historical changes in the geomagnetic field, and to further evaluate the hypothesis of periodic flux expulsion, we presented archaeomagnetic data from southern Africa which extend the existing directional curve back to the first millennium. The data record a second earlier episode of rapid directional change, and define a loop which is absent from CALS3k.4. The coherence with archeomagnetic field models, and other regional data supports a global origin for these phenomena, which is most likely periodic Southern Hemisphere flux expulsion. Futher modelling, as well as archaeointensity analyses from these materials, will help to shed light on the timing of these episodes, and to further constrain the dynamics of core processes. We briefly note that the improved resolution offered by our record raises the possibility of archaeomagnetic dating in this region.

**Author Contributions:** J.A.T., T.H., M.W., P.C.T. and M.M. conducted field collections, R.D.C. and V.J.H conducted and supervised sample preparation and laboratory measurements, and analyzed magnetic data together with J.A.T. V.J.H. and R.K.B. analyzed geomagnetic model predictions, and V.J.H. recognized the correlation with geomagnetic jerks. V.J.H. wrote the first draft of the manuscript and received subsequent contributions from the coauthors. J.A.T conceived the project with T.H. and M.W. and supervised the overall investigation. New data presented here is available in the Earthref (MagIC) database, http://earthref.org/MagIC/16376

#### Acknowledgments

274

281

- This research was supported by NSF Grant EAR-1448227 to J. A. Tarduno. Excavation
- was conducted under permits from the South African Heritage Resources Agency. Several
- students helped with field collection: Susanana Chhibber, Sebastian Fearn, Shiri Goldman-
- Nedergaard, Timothy O'Brien, and Hannah Tompkins. Monika Korte kindly provided
- spherical harmonic coefficients for the CALS3k.4 and ARCH3k.1 models. We thank the
- anonymous reviewers for their helpful comments.

## References

- Amerigian, C., Watkins, N. D. and Ellwood, B. B., 1974. Brunhes epoch geomagnetic sec-
- ular variation on Marion island: Contribution to evidence for a long-term regional geo-
- magnetic secular variation maximum. J. Geomagn. Geoelectr. 26, 429–441.
- <sup>285</sup> Cottaar, S. and Lekic, V., 2016. Morphology of seismically slow lower-mantle structures.
- Geophys. J. Int. 207, 1122–1136.
- Day, R., Fuller, M., and Schmidt, V.A. 1977. Hysteresis properties of titanomagnetites:
- Grain size and composition dependence. Physics of the Earth and Planetary Interiors 13,
- 260-267.
- De Santis, A., Qamili, E., 2008. Are we going towards a global planetary magnetic
- change? 1st WSEAS International Conference on "Environmental and Geological Sci-
- ence and Engineering (EG'08)". World Scientific and Engineering Academy and Society
- Press.
- Donadini, F., Serneels, V., Kapper, L. and El Kateb, A., 2015. Directional changes of the
- geomagnetic field in West Africa: Insights from the metallurgical site of Korsimoro.
- 296 Earth Planet. Sc. Lett. 430, 349–355.
- Dumberry, M. and Finlay, C. C., 2007. Eastward and westward drift of the Earth's mag-
- netic field for the last three millennia. *Earth Planet. Sc. Lett.* 254, 146–157.
- Dunlop, D.J. 2002. Theory and application of the Day plot  $(M_{rs}/M_s \text{ versus } H_{cr}/H_c)$  1.
- Theoretical curves and tests using titanomagnetite data. Journal of Geophysical Research
- 107, EPM4-1–EPM4-22.
- Fisher, R., 1953. Dispersion on a sphere. *P. Roy. Soc. A Math. Phy.* 217, 295–305.
- Gallet, Y., Genevey, A. and Le Goff, M., 2002. Three millennia of directional variation
- of the Earth's magnetic field in western Europe as revealed by archeological artefacts.
- 305 Phys. Earth Planet. In. 131, 81–89.

- Gallet, Y., Genevey, A. and Courtillot, V., 2003. On the possible occurrence of 'archaeo-
- magnetic jerks' in the geomagnetic field over the past three millennia. Earth Planet. Sc.
- 308 Lett. 214, 237–242.
- Gallet, Y., Hulot, G., Chulliat, A. and Genevey, A., 2009. Geomagnetic field hemispheric
- asymmetry and archeomagnetic jerks. Earth Planet. Sc. Lett., 284, 179–186.
- Gubbins, D., Jones, A. L. and Finlay, C. C., 2006. Fall in Earth's magnetic field is erratic.
- 312 Science 312, 900–902.
- Huffman, T.N. 1978. The Iron Age of the Buhwa District, Rhodesia. Occasional Papers
- National Museums Rhodesia A 4(3), 2–22.
- Huffman, T.N., 2007. Handbook to the Iron Age: The Archaeology of Pre-colonial Farm-
- ing Societies in Southern Africa. University of KwaZulu-Natal Press, South Africa.
- Huffman, T.N., 2009. A cultural proxy for drought: ritual burning in the Iron Age of
- southern Africa. J. Archaeol. Sci. 36, 991–1005.
- Huffman T.N. and du Piesanie, J. 2011. Khami and the Venda in the Mapungubwe land-
- scape. Journal of African Archaeology 9 (2), 189-206.
- Huffman, T.N., Elburg, M. and Watkeys, M. 2013. Vitrified cattle dung in the Iron Age of
- Southern Africa. Journal of Archaeological Science 40, 3553-3560.
- Huffman, T. N. and Woodborne, S., 2016. Archaeology, baobabs and drought: Cultural
- proxies and environmental data from the Mapungubwe landscape, southern Africa. The
- 325 Holocene 26, 464–470.
- Huffman, T.N., Thebe, P.C., Watkeys, M.K. and Tarduno, J. 2016. Archaeo-metallurgy in
- the Tswapong Hills; a preliminary report on archaeological context. Southern African
- 328 *Humanities* 28, 119-133.
- Hulot, G., Eymin, C., Langlais, B., Mandea, M. and Olsen, N., 2002. Small-scale structure
- of the geodynamo inferred from Oersted and Magsat satellite data. *Nature* 416, 620-
- 331 623.
- Jackson, A., Jonkers, A.R. and Walker, M.R., 2000. Four centuries of geomagnetic secular
- variation from historical records. *P. Roy. Soc. A Math. Phy.* 358, 957–990.
- Kapper, L., Donadini, F., Serneels, V., Tema, E., Goguitchaichvili, A. and Morales, J. J.,
- 2017. Reconstructing the geomagnetic field in west Africa: First absolute intensity re-
- sults from Burkina Faso. Sci. Reports 7: 45225.
- Kirschvink, J. L. 1980. The least-squares line and plane and the analysis of palaeomag-
- netic data. *Geophys. J. Int.* 62, 699-718.

- Korte, M., Donadini, F. and Constable, C.G., 2009. Geomagnetic field for 0–3 ka: 2. A
- new series of time-varying global models. Geochem., Geophy., Geosy. 10.
- Korte, M. and Constable, C., 2011. Improving geomagnetic field reconstructions for 0-
- 3ka. Phys. Earth Planet. In. 188, 247–259.
- Laj, C. and Kissel, C., 2015. An impending geomagnetic transition? Hints from the past.
- *Front. Earth Sci.* 3, 61.
- Lekic, V., Cottaar, S., Dziewonski, A. and Romanowicz, B., 2012. Cluster analysis of
- global lower mantle tomography: A new class of structure and implications for chem-
- ical heterogeneity. Earth Planet. Sc. Lett. 357, 68–77.
- Licht, A., Hulot, G., Gallet, Y. and Thébault, E., 2013. Ensembles of low degree archeo-
- magnetic field models for the past three millennia. *Phys. Earth Planet. In.* 224, 38–67.
- Main, M. 2002. Tswapong Hills, Report, Archaeological Surveys 1996 2002. On file,
- National Museums and Art Gallery, Gaborone.
- Main, M. 2008.Report on Tswapong Hills archaeological surveys 1996-2002. Botswana
- Notes and Records 40, 55-59.
- Mitra, R., Tauxe, L. and McIntosh, S. K., 2013. Two thousand years of archeointensity
- from West Africa. Earth Planet. Sc. Lett. 364, 123–133.
- Neukirch, L. P., Tarduno, J. A., Huffman, T. N., Watkeys, M. K., Scribner, C. A. and Cot-
- trell, R. D., 2012. An archeomagnetic analysis of burnt grain bin floors from ca. 1200
- to 1250 AD Iron-Age South Africa. Phys. Earth Planet. In. 190, 71-79.
- Nilsson, A., Holme, R., Korte, M., Suttie, N. and Hill, M., 2014. Reconstructing Holocene
- geomagnetic field variation: new methods, models and implications. Geophys. J. Int.,
- p.ggu120.
- Pavón-Carrasco, F. J., Osete, M. L. and Torta, J. M., 2010. Regional modeling of the
- geomagnetic field in Europe from 6000 to 1000 BC. Geochem., Geophy., Geosy. 11,
- Q11008, doi:10.10292010GC003197.
- Pavón-Carrasco, F. J., Osete, M. L., Torta, J. M. and De Santis, A., 2014. A geomag-
- netic field model for the Holocene based on archaeomagnetic and lava flow data. Earth
- Planet. Sci. Int. 388, 98–109, doi:10.1029j.epsl.2013.11.046.
- Pavón-Carrasco, F. J. and De Santis, A., 2016. The South Atlantic Anomaly: The key for
- a possible geomagnetic reversal. Front. Earth Sci. 4, 40.
- Pike, C. R., Roberts, A. P., Verosub, K. L., 1999. Characterizing interactions in fine mag-
- netic particle systems using first order reversal curves. J. Appl. Phys. 85, 6660–6667.

- Robinson, K.R. 1961. An Early Iron Age site from the Chibi District, Southern Rhodesia.
- South African Archaeological Bulletin 16, 95-102.
- Shuey, R. T., Cole, E. R. and Mikulich, M. J., 1971. Geographic correction of archeomag-
- netic data. J. Geomagn. Geoelectr. 22, 485–489.
- Tarduno, J. A., Watkeys, M. K., Huffman, T., Cottrell, R. D., Blackman, E. G., Wendt,
- A., Scribner, C. A., Wagner, C. L., 2015. Antiquity of the South Atlantic Anomaly and
- evidence for top-down control on the geodynamo. *Nat. Commun.* 6.
- Tema, E. and Kondopoulou, D., 2011. Secular variation of the Earth's magnetic field in
- the Balkan region during the last eight millennia based on archaeomagnetic data. Geo-
- *phys. J. Int.* 186, 603–614.
- Terra-Nova, F., Amit, H., Hartmann, G.A., Trindade, R.I. and Pinheiro, K.J., 2017. Relat-
- ing the South Atlantic Anomaly and geomagnetic flux patches. Phys. Earth Planet. In.
- 266, 39–53.
- Wündsch, M., Haberzettl, T., Meadows, M. E., Kirsten, K. L., Kasper, T., Baade, J.,
- Daut, G., Stoner, J. S. and Mäusbacher, R., 2016. The impact of changing reservoir ef-
- fects on the 14C chronology of a Holocene sediment record from South Africa. Quat.
- 388 *Geochronol.* 36, 148–160.

**Table 1.** Mean archaeomagnetic directions and fit statistics obtained for southern Africa. N'/N, number of specimens from locality used in analysis/number of specimens measured; D ( $^{o}$ ) mean declination; I ( $^{o}$ ) mean inclination; k, an estimate of the dispersion of the population of directions;  $\alpha_{95}$ , confidence limit for n number of directions. See main text and Tables S1-S8 for more information.

Locality	Age CE	N'/N	D (°)	I (°)	k	α <sub>95</sub> (°)
Faure Ruins (FR)	1500–1610	11/12	352.4	-35.8	39	7.4
Rhino Mine I (RME)	750–800	17/25	21.7	-22.4	73	4.2
Mabveni (MB)	675–700	17/18	11.8	-16.7	76	4.1
Manong East (ME)	590-636	26/32	10.3	-23.7	101	2.8
Rhino Mine II (RME)	550-570	13/13	3.0	-29.9	80	4.7
Buhwa (SL)	400–450	19/36	2.7	-38.3	60	4.4

**Figure 1.** Location of sites presented in this study (a), showing new localities (green triangles), and previous studies (red circles, *Neukirch et al.* [2012]; *Tarduno et al.* [2015]). Yellow star shows the coordinates of Mapungubwe (22.212 °S, 29.387 °E). Photograph of *in situ* floor from site RME1 (b) is shown along with examples of excavated fragments (c). Each fragment sampled has a unique field orientation line recorded by Brunton and Sun compasses.

**Figure 2.** Characterization of rock magnetic mineralogy for fragment RME4-5. (a) Bulk magnetic susceptibility (K) versus temperature plotted for heating (red) and cooling (blue). (b) Magnetic hysteresis curve and fitted parameters, and (c) first order reversal curve (FORC) diagram for the same sample generated using FORCinel v2.03 with a smoothing factor of 3 and first point artifact removed.  $M_r$ , saturation remanent magnetization;  $M_s$ , saturation magnetization;  $H_c$ , coercivity;  $H_{cr}$ , coercivity of remanence. Note slight wasp-waisted curve.

Figure 3. Typical orthogonal vector demagnetization plots showing behavior during AF demagnetizations

(a-c) and thermal demagnetizations (d-f). AF steps are annotated in mT and thermal steps are annotated in

OC. Declination and inclination are presented as filled blue circles and open red squares, respectively. (For

interpretation of the references to colour in this figure, the reader is referred to the web version of this article.)

Figure 4. Stereonet of archaeomagnetic directional data from southern Africa [this study, previous work of

Neukirch et al. [2012] (198, AD300), Tarduno et al. [2015] (KL, AD160, AD6)], plotted with 95% confidence

ellipses. All directions are reduced to the geographic coordinates of Mapungubwe (22.212 °S, 29.387 °E).

Dashed black line shows field evolution from 1650 CE to the present according to CALS3k.4 [Korte and

Constable, 2011]. Green arrows show rates of change defined by the directional data (see text, SI Table S8)

Figure 5. Comparison of Southern Africa paleomagnetic and archeomagnetic data of this study, combined with the data of *Neukirch et al.* [2012] and *Tarduno et al.* [2015], to the predicted geomagnetic field of five published field models. Paleomagnetic/archeomagnetic and field model predicted directions are reduced to a common site location (Mapungubwe: 22.212 °S, 29.387 °E). Color scale denotes age of data and corresponding model age values. Curve connecting site data is drawn for visual aid. (a) Stereonet projection of predicted geomagnetic field directions using the A\_FM model [*Licht et al.*, 2013] for 400 to 1600 CE and paleomagnetic/archeomagnetic directional data for Southern Africa during that interval. (b) PFM9k geomagnetic field model of *Nilsson et al.* [2014]. (c) CALS3k.4 [*Korte and Constable*, 2011]. (d) ARCH3k.1(MAST) [*Korte et al.*, 2009]. (e) SHA\_DIF\_14K [*Pavón-Carrasco et al.*, 2014]. (f) Ratio of quadrupole to dipole energy components ((Q)/(D)) evolution over time using three geomagnetic field models (following *Gallet et al.* [2009]). Red dashed line: ARCH3k.1(MAST) [*Korte et al.*, 2009]; blue dashed line: A\_FM [*Licht et al.*, 2013]; green dashed line: SHA\_DIF\_14K [*Pavón-Carrasco et al.*, 2014]. Arrows show periods of archeomagnetic jerks in the archeointensity record [*Gallet et al.*, 2009]. Thick black bars show rates for changes of field direction observed in the paleomagnetic/archeomagnetic data for Southern Africa. Arrows are times of geomagnetic jerks as proposed by *Gallet et al.* [2009].

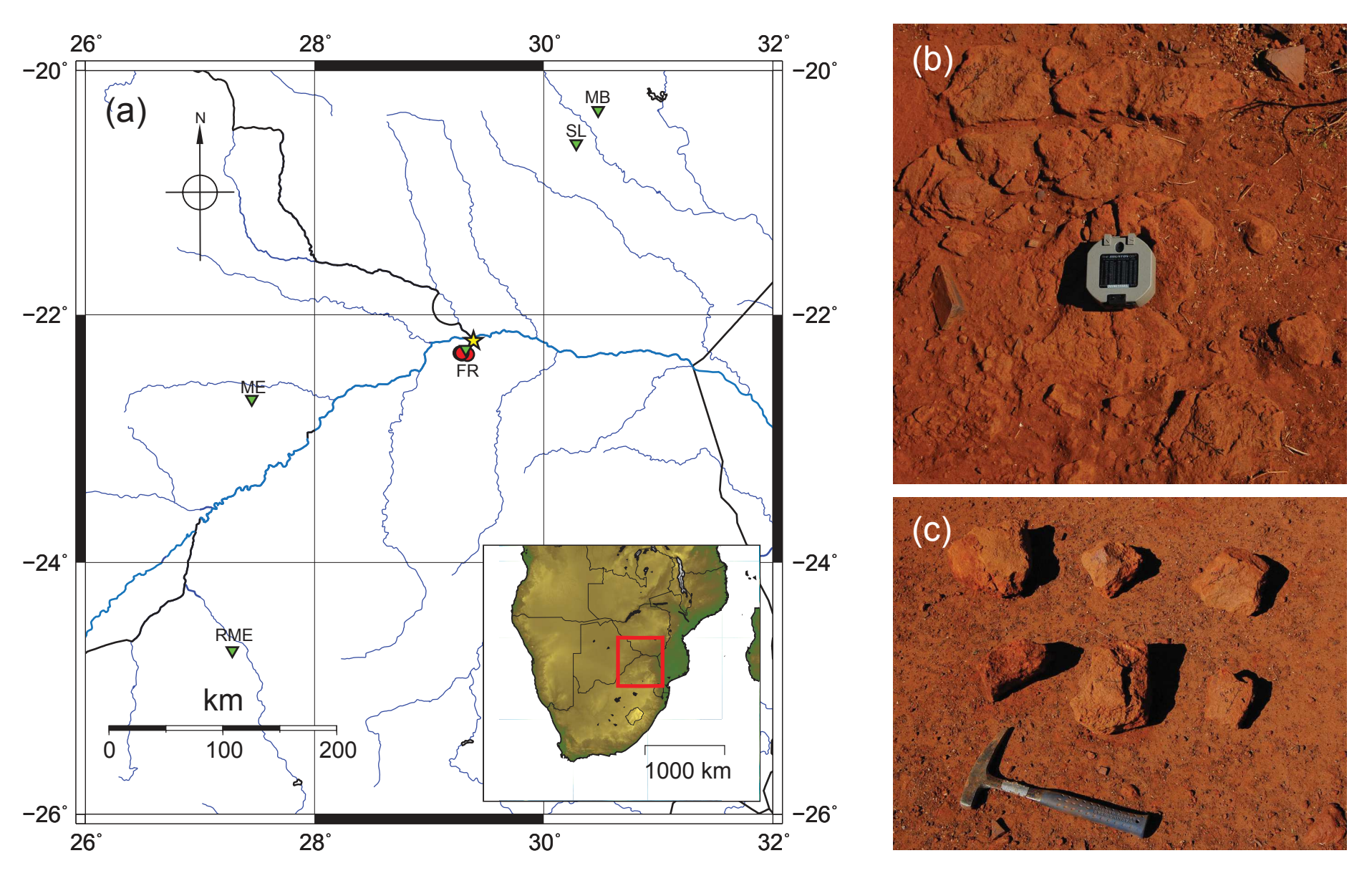


Figure 1

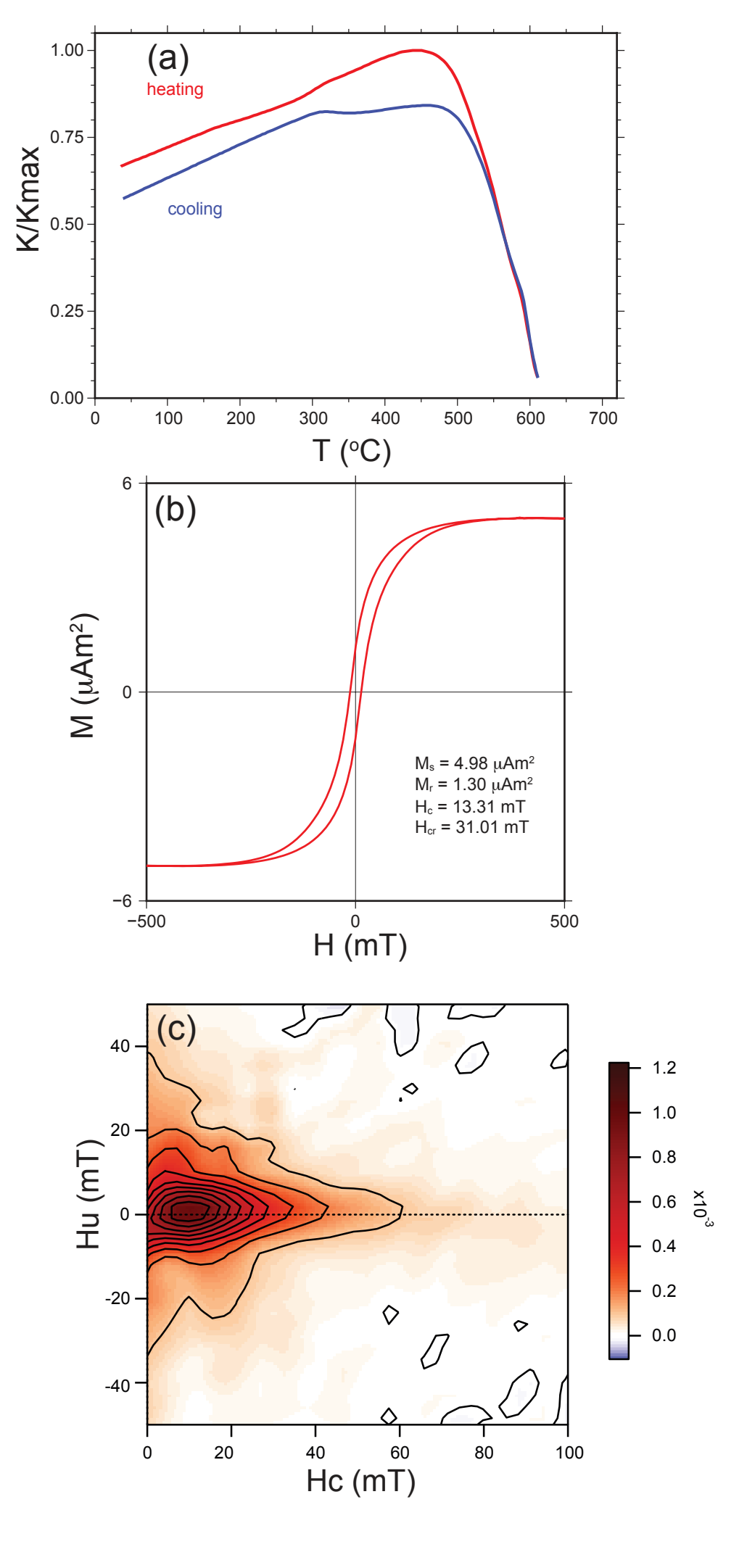


Figure 2

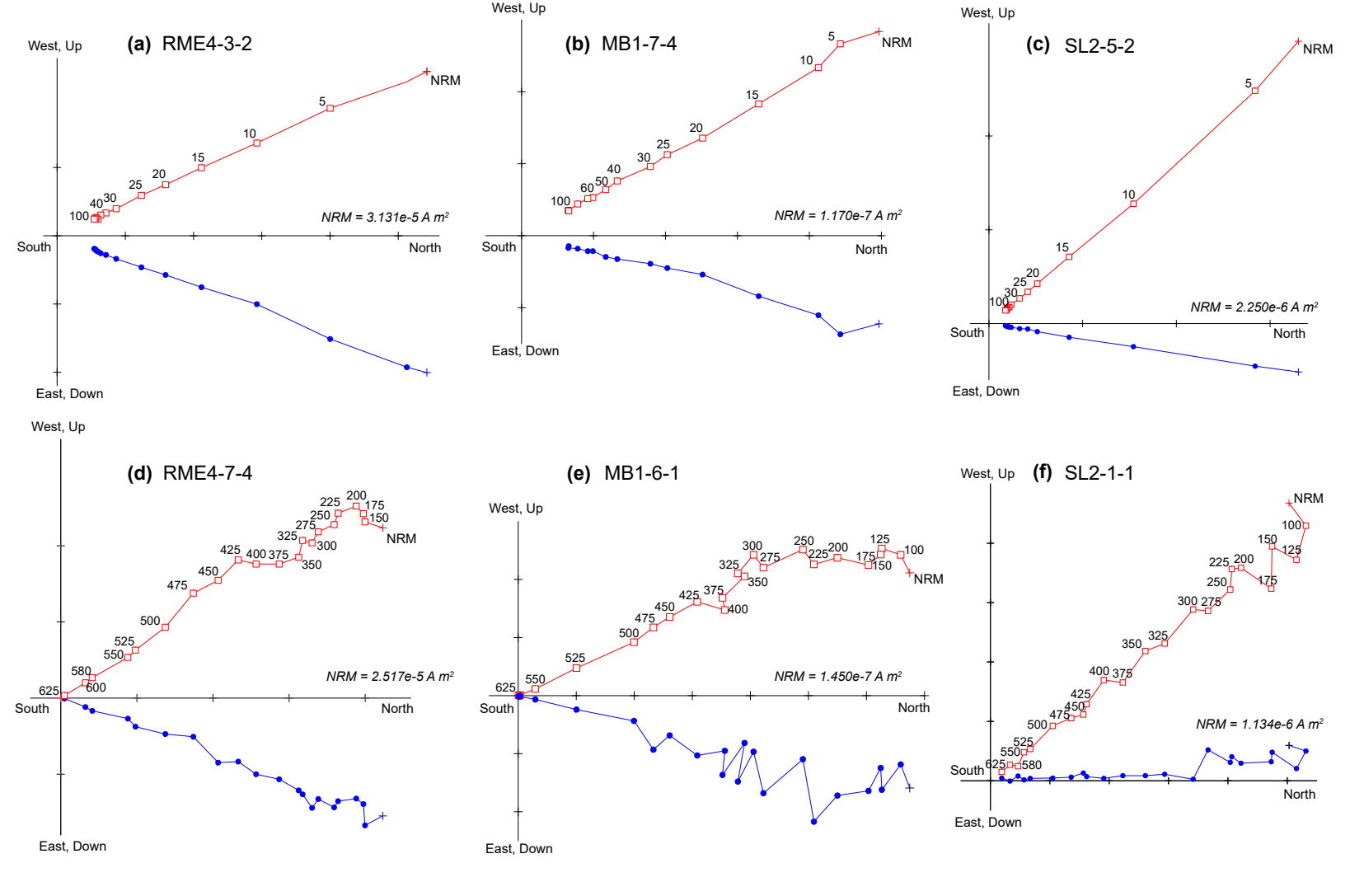
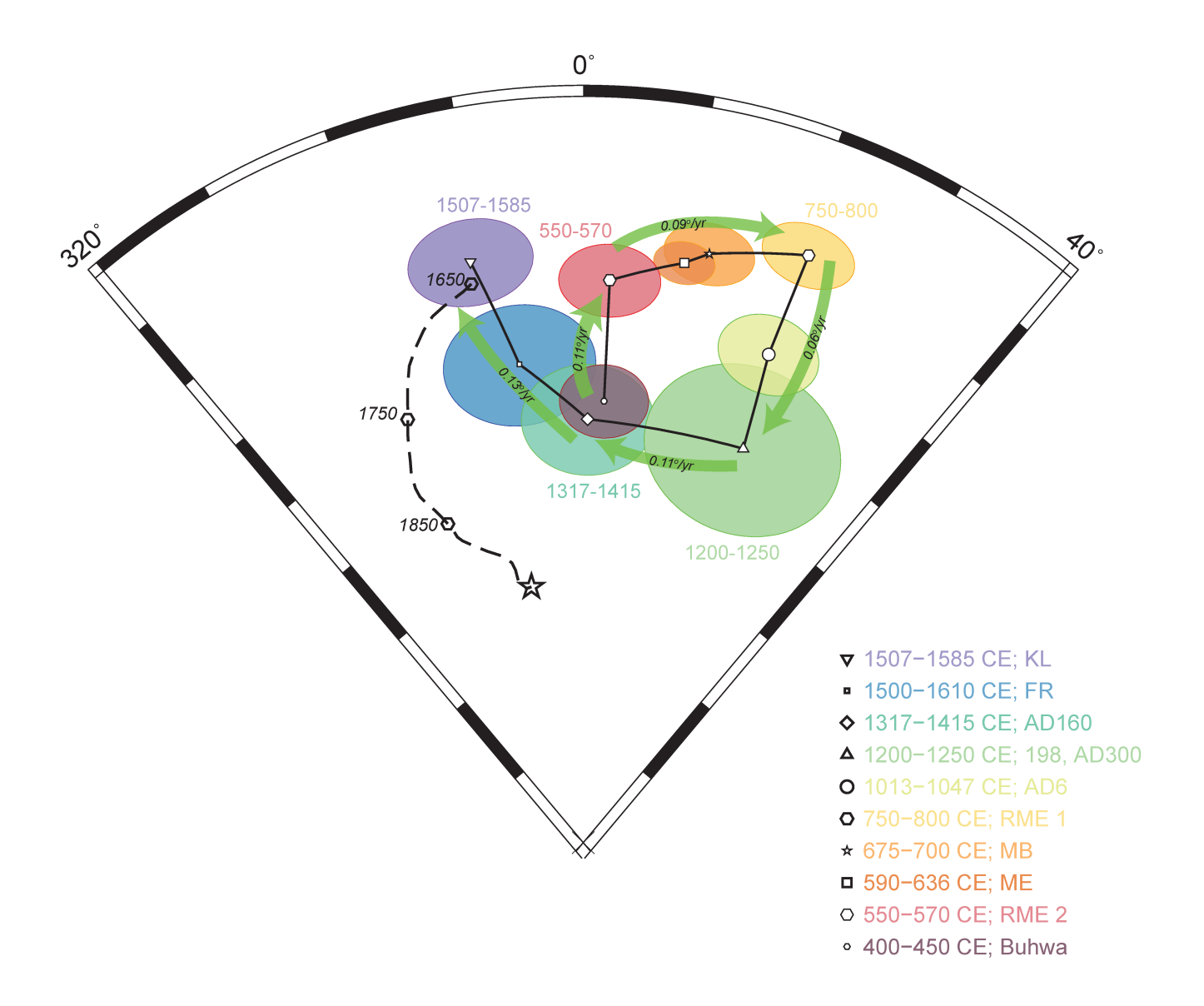


Figure 3



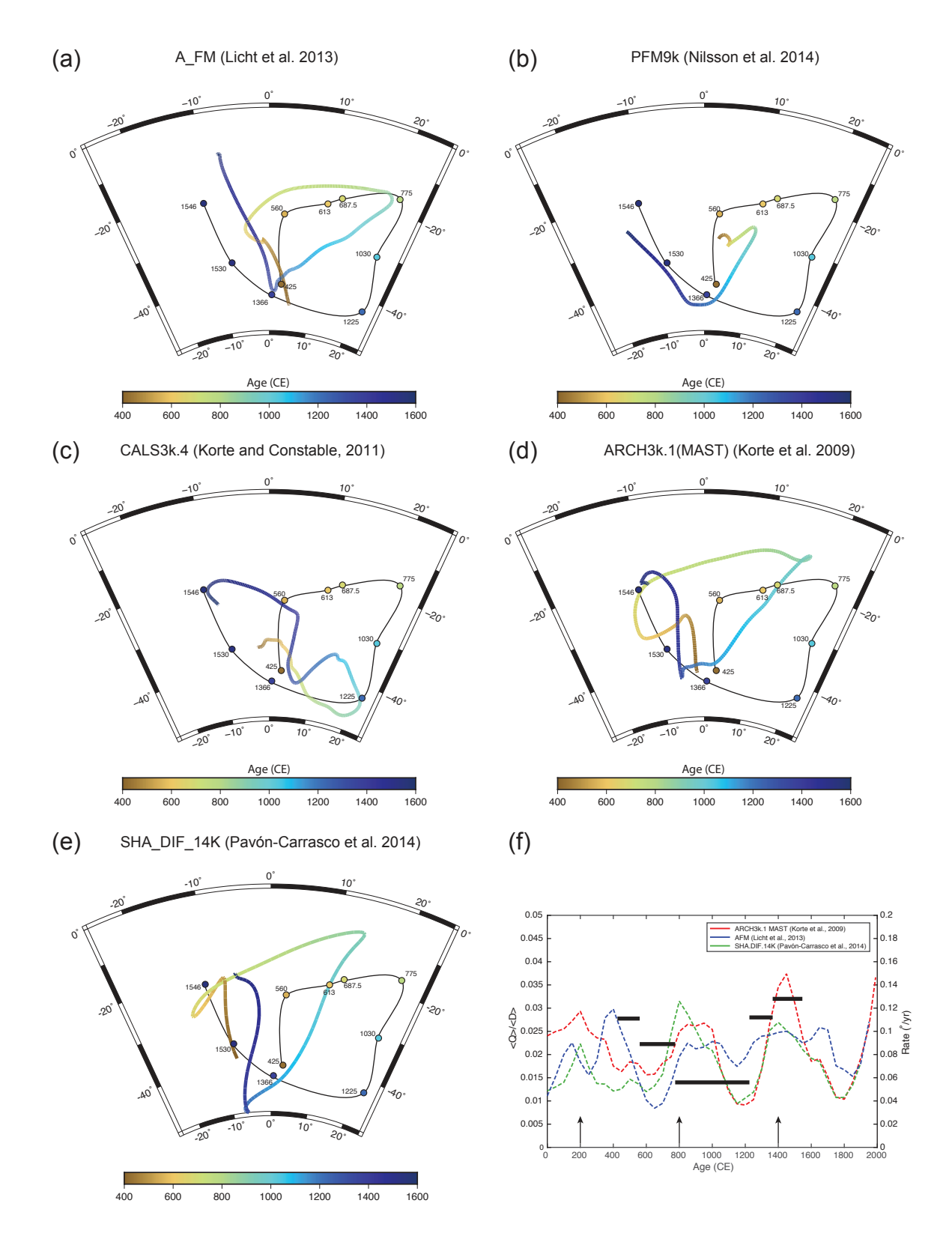


Figure 5

# **Supporting Information for**

"New archeomagnetic directional records from Iron-Age southern Africa (ca. 425–1550 CE) and implications for the South Atlantic Anomaly"

Vincent J. Hare<sup>1</sup>, John A. Tarduno<sup>1,2,3</sup>, Thomas Huffman<sup>4</sup>, Michael Watkeys<sup>3</sup>, Phenyo C. Thebe<sup>5</sup>, Munyaradzi Manyanga<sup>6</sup>, Richard K. Bono<sup>1</sup>, Rory D. Cottrell<sup>1</sup>

Department of Earth and Environmental Sciences, University of Rochester, Rochester, New York 14627, USA
 Department of Physics and Astronomy, University of Rochester, Rochester, New York 14627, USA
 School of Geological Sciences, University of KwaZulu-Natal, Durban 4000, South Africa
 School of Geography, Archaeology and Environmental Studies, University of the Witwatersrand, Johannesburg 2050,

South Africa

<sup>5</sup> Archaeology Unit, Department of History, University of Botswana, Gaborone 0022, Botswana

<sup>6</sup> History Department, University of Zimbabwe, Harare, Zimbabwe

# **Contents**

- 1. Sampling Hierarchy, Figure S1
- 2. Tables S1 to S8
- 3. Figures S2 to S7
- 4. Outlier Procedure
- 5. Model Comparisons
- 6. Description of archaeological sites and age constraints

Corresponding author: Rory D. Cottrell, rory.cottrell@rochester.edu

## 1. Sampling Hierarchy

At each locality (e.g. Faure Ruins, FR; level 1), burnt structures (in this case, kraal) are collected; the number of structures collected is dependent on availability as determined by the archeologists. Each burnt structure is assigned as a site (e.g. FR1, FR2, FR3; level 2). From each site, one or more fragments (e.g., FR1-1, FR1-2, etc.; level 3) are oriented in the field with Sun and Brunton compasses (see Figure 1b) and marked by an arrow before they are removed from in situ positions (see Figure 1c). The number of fragments vary at a site based on availability. In the lab, the orientation line on each fragment is transferred as a series of parallel lines (on the orientation surface) and orthogonal lines (orthogonal to the orientation plane as defined by the arrow drawn in the field) before cutting with a bronze blade into a series of specimens (e.g. FR1-1-3; level 4).

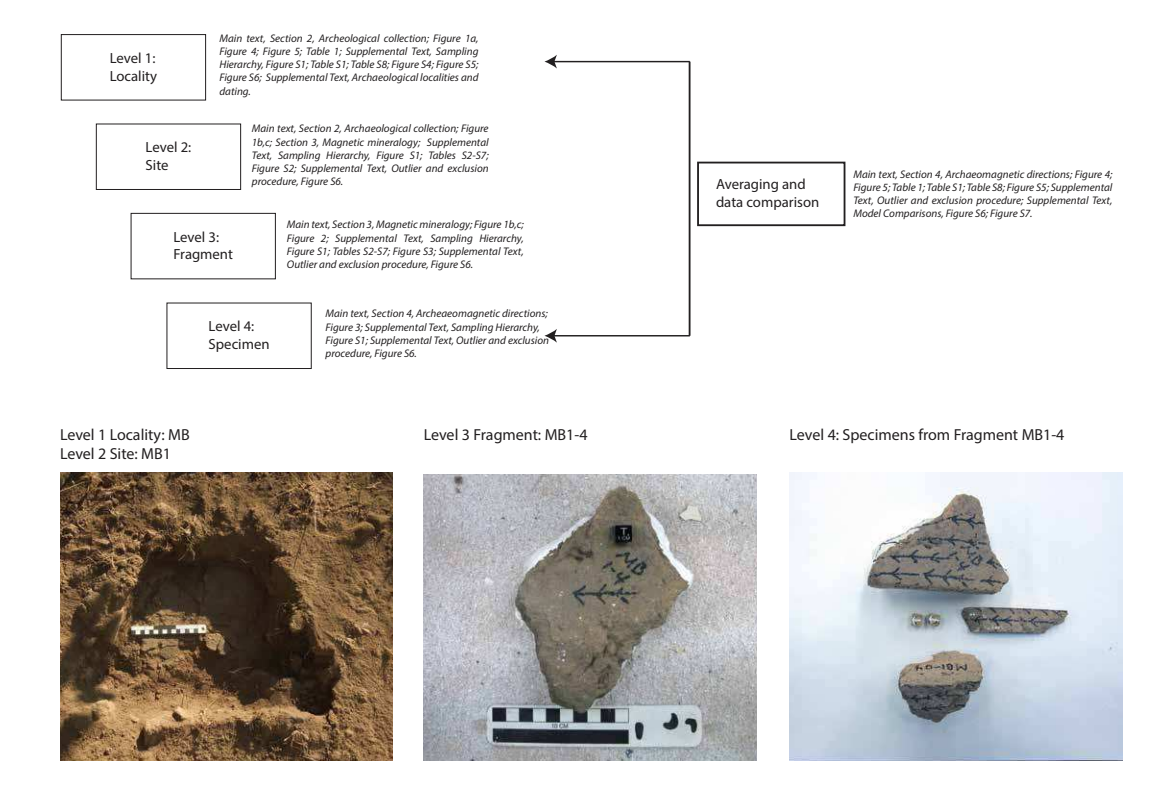


**Figure S1.** Hierarchy of sampling, with index to where data are presented and discussed in this manuscript, with MB locality shown as an example.

# 2. Supporting Information Tables

**Table S1.** Summary paleomagnetic directional data. Locality; Site Identifying name (ID); archeological material (Type); N', number of samples used in the analyses; Sites, number of independent time units presented; Dec, declination; Inc, inclination; k, estimate of the precision parameter;  $\alpha_{95}$ , confidence interval. Italicized entries are preferred values for directional analysis presented here.

Locality	ID	Type	Age (cal CE)	N'	Sites	Dec (°)	Inc (°)	k	$\alpha_{95}  (^{o})$
Kolope‡	KLA,B	hutfloor, kraal	1507–1585	18	2	349.0	-22.0	1937	5.7
Faure Ruins	FR1	kraal	1500-1610	4	1	352.7	-31.3	62	11.8
Faure Ruins	FR2	kraal	1500-1610	3	1	8.0	-48.6	387	6.3
Faure Ruins	FR3	kraal	1500-1610	4	1	349.6	-30.1	77	10.5
Faure Ruins Mean			1500-1610	11		352.4	-35.8	39	7.4
Icon (Venetia)‡	AD160	kraal	1317–1415	14	1	0.6	-42.9	37	6.6
AD300†	AD300, AD198A,B	grain bin	1200-1250	28	3	22.1	-42.8	152	10.0
Baobab‡	AD6A,B,C	grain bin	1013–1047	47	3	20.8	-31.0	602	4.9
Rhino Mine	RME1	grain bin	750-800	11	1	21.2	-21.9	58	6.1
Rhino Mine	RME4	grain bin	750-800	6	1	22.5	-23.3	116	6.3
Rhino Mine I Mean			750–800	17		21.7	-22.4	73	4.2
Mabveni Mean	MB1	grain bin	675–700	17	1	11.8	-16.7	76	4.1
Manong East	ME1	hut floor	590-636	15	1	12.2	-22.2	129	3.4
Manong East	ME2	hut floor	590-636	11	1	7.6	-25.9	92	4.8
Manong East Mean			590–636	26		10.3	-23.7	101	2.8
Rhino Mine II Mean		grain bin	550–750	13	1	3.0	-29.9	80	4.7
Buhwa	SL1	grain bin	400–450	13	1	340.7	-19.3	15	8.8
Buhwa	SL2	grain bin	400–450	19	1	2.7	-38.3	60	2.9
Buhwa Mean			400-450	19		2.7	-38.3	60	4.4

Previously published value. See  $\dagger$ Neukirch et al. (2012) and  $\ddagger$ Tarduno et al. (2015) for details.

**Table S2.** Paleomagnetic directional data. AF, alternating field demagnetization, Th, thermal demagnetization; Steps, demagnetization steps used in principal component analysis (PCA), +0, origin used in PCA fit;  $N_p$ , number of steps used in PCA fit; MAD, maximum angular deviation of PCA fit.

Locality	Specimen	Method	Steps	$N_p$	Dec (°)	Inc (°)	MAD (°)
Faure Ruins	FR1-1-3	AF	p15.0-60.0+0	8	353.8	-35.1	6.5
	FR1-1-2	AF	p20.0-100.0+0	11	0.6	-41.4	3.3
	FR1-2-2	AF	p15.0-60.0+0	8	347.2	-20.0	3.2
	FR1-2-3	AF	p25.0-100.0+0	10	350.8	-28.3	3.3
	FR2-1-2	AF	p30.0-100.0+0	9	9.2	-44.5	2.9
	FR2-1-3	AF	p25.0-100.0+0	10	6.0	-48.8	2.3
	FR2-1-4	Th	p325.0-550.0+0	11	8.8	-52.4	18.5
	FR2-2-3‡	AF	p15.0-100.0+0	12	315.9	-48.3	1.7
	FR3-1-2	AF	p20.0-100.0+0	11	1.3	-31.1	1.5
	FR3-1-3	AF	p30.0-100.0+0	9	354.9	-31.2	2.4
	FR3-2-3	AF	p70.0–100.0+0	5	344.4	-25.5	7.5
	FR3-2-4	Th	p275.0-450.0+0	9	338.7	-31.4	20.5

<sup>‡:</sup> outlier removed from final analysis (further details may be found in Section 3, this Supplementary Information). The sampling code, e.g. "FR-A-B-C" is as follows: "FR", locality; "A", site, "B" fragment; "C", specimen.

**Table S3.** Paleomagnetic directional data (continued). Sampling codes, abbreviations and symbols used are the same convention as Table S2.

Locality	Specimen	Method	Steps	$N_p$	Dec (°)	Inc (°)	MAD (°)
Rhino Mine I	RME1-1-1‡	AF	p15.0-100.0+0	12	8.2	-8.4	1.4
	RME1-1-2‡	AF	p20.0-100.0+0	12	4.4	-10.8	1.7
	RME1-2-2‡	AF	p25.0-100.0+0	11	1.1	-24.5	2.9
	RME1-2-5	AF	p25.0-100.0+0	10	6.6	-26.4	1.9
	RME1-3-1	AF	p20.0-100.0+0	13	13.2	-24.9	2.0
	RME1-3-3	AF	p15.0-40.0+0	6	16.3	-20.4	1.3
	RME1-4-1	AF	p20.1-100.0+0	11	13.2	-27.4	1.1
	RME1-4-4‡	AF	p20.1-100.0+0	11	2.5	-34.7	1.1
	RME1-5-3	AF	p20.1-100.0+0	11	33.5	-11.0	1.3
	RME1-5-4	AF	p25.0-100.0+0	10	32.6	-10.8	1.6
	RME1-6-2	AF	p20.1-100.0+0	11	22.6	-18.5	1.8
	RME1-6-4	AF	p15.0-100.0+0	12	20.5	-17.4	1.5
	RME1-6-6	Th	p475.0-525.0+0	7	27.5	-31.6	3.0
	RME1-7-1	AF	p35.0-100.0+0	8	28.0	-30.0	1.8
	RME1-8-1‡	AF	p20.0-100.0+0	11	12.5	-45.7	0.7
	RME1-12-1‡	AF	p20.0-100.0+0	11	4.0	-18.6	1.0
	RME1-13-1	AF	p20.0-100.0+0	11	17.8	-19.7	1.1
	RME4-2-1	AF	p15.0-40.0+0	6	27.2	-24.4	1.2
	RME4-3-2	AF	p20.0-100.0+0	11	19.6	-24.2	1.4
	RME4-5-2	AF	p20.0-100.0+0	11	16.9	-18.6	1.7
	RME4-6-2	AF	p50.0–100.0+0	6	19.0	-18.0	3.1
	RME4-7-3	AF	p15.0–100.0+0	12	31.6	-21.2	4.6
	RME4-7-4	Th	p375.0-525.0+0	8	20.8	-32.8	6.4
	RME4-8-2‡	AF	p20.0-100.0+0	11	44.0	-29.1	1.8
	RME4-8-3‡	Th	p425.0–550.0+0	7	35.9	-24.9	5.0

<sup>‡:</sup> outlier removed from final analysis (further details may be found in Section 3, this Supplementary Information). The sampling code, e.g. "RME-A-B-C" is as follows: "RME", locality; "A", site, "B" fragment; "C", specimen.

**Table S4.** Paleomagnetic directional data (continued). Sampling codes, abbreviations and symbols used are the same convention as Table S2.

Locality	Specimen	Method	Steps	$N_p$	Dec (°)	Inc (°)	MAD (°)
Mabveni	MB1-1-2	AF	p30.0-70.0+0	6	15.9	-22.2	1.8
	MB1-1-3	AF	p30.0-100.0+0	9	17.1	-23.6	2.1
	MB1-1-4	AF	p30.0-100.0+0	9	17.0	-22.0	1.8
	MB1-2-1‡	Th	p450.0-580+0	7	12.8	0.2	2.3
	MB1-2-2	AF	p20.0-100.0+0	11	12.1	-3.1	2.5
	MB1-2-3	AF	p30.0-100.0+0	9	10.4	-4.2	3.1
	MB1-2-4	AF	p25.0-100.0+0	10	7.4	-7.2	2.4
	MB1-3-1	Th	p450.0-580.0+0	7	5.0	-11.3	0.6
	MB1-3-2	AF	p40.0-100.0+0	8	6.4	-7.9	3.1
	MB1-3-3	AF	p25.0-100.0+0	10	5.8	-9.3	1.6
	MB1-4-1	AF	p30.0-100.0+0	9	19.7	-13.6	1.7
	MB1-4-3	AF	p25.0-100.0+0	10	13.3	-13.3	3.3
	MB1-6-1	Th	p425-580+0	8	17.9	-26.3	4.7
	MB1-6-2	AF	p25.0-100.0+0	10	11.0	-22.3	1.6
	MB1-6-3	AF	p60.0-100.0+0	6	12.7	-22.7	3.2
	MB1-7-2	AF	p60.0-100.0+0	6	8.8	-22.7	1.9
	MB1-7-3	AF	p40.0-100.0+0	8	8.2	-23.2	2.6
	MB1-7-4	AF	p25.0-100.0+0	10	12.5	-28.3	1.6

<sup>‡:</sup> outlier removed from final analysis (further details may be found in Section 3, this Supplementary Information). The sampling code, e.g. "MB-A-B-C" is as follows: "MB", locality; "A", site, "B" fragment; "C", specimen.

**Table S5.** Paleomagnetic directional data (continued). Sampling codes, abbreviations and symbols used are the same convention as Table S2.

Locality	Specimen	Method	Steps	$N_p$	Dec (°)	Inc (°)	MAD (°)
Manong East	ME1-1-1	Th	p475-550+0	5	11.9	-21.7	5.9
	ME1-1-2	AF	p60.0-100.0+0	6	4.2	-18.1	3.3
	ME1-1-3‡	AF	p50.0-100.0+0	7	6.2	-17.5	1.9
	ME1-2-1	Th	p475.0-550.0+0	5	8.2	-25.7	5.4
	ME1-2-2	AF	p40.0-100.0+0	8	8.6	-20.2	3.0
	ME1-2-3	AF	p40.0-100.0+0	7	6.2	-17.5	1.9
	ME1-3-1	Th	p450.0-550.0+0	6	17.2	-20.3	5.5
	ME1-3-2	AF	p25.0-100.0+0	10	15.1	-16.7	2.2
	ME1-3-3	AF	p40.0-100.0+0	8	17.9	-17.8	1.6
	ME1-4-2	AF	p25.0-100.0+0	10	3.5	-21.3	2.7
	ME1-4-3‡	AF	p25.0-100.0+0	10	355.0	-17.5	2.7
	ME1-5-1	Th	p475.0-600.0+0	8	10.5	-22.2	4.1
	ME1-5-2	AF	p25.0-100.0+0	10	9.6	-32.9	2.8
	ME1-5-3	AF	p40.0-100.0+0	8	11.7	-16.7	5.2
	ME1-6-1	Th	p375.0-600.0+0	13	18.6	-28.2	3.4
	ME1-6-2	AF	p30.0-100.0+0	9	21.0	-25.8	4.3
	ME1-6-3	AF	p25.0-100.0+0	10	19.9	-26.7	3.6
	ME2-1-2	AF	p40.0-100.0+0	8	4.1	-37.1	3.9
	ME2-1-3	AF	p60.0-100.0+0	6	8.2	-29.9	2.5
	ME2-2-1	Th	p425.0-600.0+0	10	2.5	-21.5	3.8
	ME2-2-2‡	AF	p40.0-100.0+0	8	356.1	-18.8	1.2
	ME2-2-3	AF	p40.0-100.0+0	8	0.0	-22.5	3.2
	ME2-3-1	Th	p375-500+0	7	19.0	-30.3	14.1
	ME2-3-2	AF	p30.0-100.0+0	9	13.2	-29.7	2.4
	ME2-3-3	AF	p20.0-100.0+0	11	13.7	-27.9	2.6
	ME2-4-2	AF	p20.0-100.0+0	11	2.2	-25.0	5.6
	ME2-4-3	AF	p20.0-100.0+0	11	0.7	-27.3	9.5
	ME2-5-2	AF	p40.0-100.0+0	8	10.3	-15.6	3.0
	ME2-5-3	AF	p50.0-100.0+0	7	10.1	-16.3	2.4
	ME2-6-2‡	AF	p25.0-100.0+0	10	28.5	-48.3	2.1
	ME2-6-3‡	AF	p25.0-100.0+0	10	21.1	-47.4	1.4
	ME2-6-4‡	AF	p30.0-100.0+0	9	16.2	-52.8	10.3

<sup>‡:</sup> outlier removed from final analysis (further details may be found in Section 3, this Supplementary Information). The sampling code, e.g. "ME-A-B-C" is as follows: "ME", locality; "A", site, "B" fragment; "C", specimen.

**Table S6.** Paleomagnetic directional data (continued). Sampling codes, abbreviations and symbols used are the same convention as Table S2.

Locality	Specimen	Method	Steps	$N_p$	Dec (°)	Inc (°)	MAD (°)
Rhino Mine II	RME2-1-1	AF	p40.0-100.0+0	7	3.7	-25.6	0.5
	RME2-1-7	AF	p50.0-100.0+0	6	356.2	-32.0	1.7
	RME2-1-9	AF	p40.0-100.0+0	7	3.3	-32.7	2.1
	RME2-2-2	AF	p40.0-100.0+0	7	357.9	-40.8	0.5
	RME2-2-4	AF	p40.0-100.0+0	7	9.23	-32.2	1.4
	RME2-3-3	AF	p40.0-100.0+0	7	1.0	-23.5	2.1
	RME2-3-7	AF	p40.0-100.0+0	7	1.6	-19.4	0.8
	RME2-4-1	AF	p40.0-100.0+0	7	6.6	-22.8	0.6
	RME2-4-7	AF	p40.0-100.0+0	7	2.6	-23.6	3.3
	RME2-5-4	AF	p40.0-100.0+0	7	2.0	-28.2	1.8
	RME2-5-6	AF	p40.0-100.0+0	7	3.4	-20.2	2.1
	RME2-6-1	AF	p40.0–100.0+0	7	4.2	-43.7	1.6
	RME2-6-3	AF	p40.0–100.0+0	7	7.5	-43.7	1.5

<sup>‡:</sup> outlier removed from final analysis (further details may be found in Section 3, this Supplementary Information). The sampling code, e.g. "RME-A-B-C" is as follows: "RME", locality; "A", site, "B" fragment; "C", specimen.

**Table S7.** Paleomagnetic directional data (continued). Sampling codes, abbreviations and symbols used are the same convention as Table S2.

Locality	Specimen	Method	Steps	$N_p$	Dec (°)	Inc (°)	MAD (°)
Buhwa	SL1-1-1‡	AF	p20.0-100.0+0	11	336.2	-14.6	2.2
	SL1-1-3‡	AF	p15.0-100.0+0	12	337.3	-20.5	0.8
	SL1-1-4‡	AF	p15.0-100.0+0	12	336.6	-9.3	1.5
	SL1-2-1‡	Th	p475.0-550.0+0	5	11.9	-21.7	4.8
	SL1-2-2‡	AF	p15.0-100.0+0	12	20.3	-37.2	1.2
	SL1-2-3‡	AF	p10.0-100.0+0	13	21.9	-37.7	0.7
	SL1-2-4‡	AF	p20.0-100.0+0	11	21.4	-40.3	1.4
	SL1-3-2‡	AF	p15.0-100.0+0	12	338.3	27.0	1.0
	SL1-3-3‡	AF	p15.0-100.0+0	12	337.5	27.0	1.1
	SL1-4-1‡	Th	p425-580+0	8	350.8	-28.4	3.2
	SL1-4-2‡	AF	p15.0-100.0+0	12	341.2	-25.6	0.7
	SL1-4-3‡	AF	p25.0-100.0+0	10	342.0	-20.7	1.8
	SL1-4-4‡	AF	p20.0-100.0+0	11	341.9	-29.3	1.0
	SL2-1-1	Th	p375.0-580.0+0	10	3.4	-43.7	4.7
	SL2-1-2	AF	p15.0-100.0+0	12	352.2	-37.4	0.2
	SL2-1-3	AF	p20.0-100.0+0	11	0.0	-37.4	0.9
	SL2-1-4	AF	p15.0-100.0+0	12	3.7	-37.7	0.7
	SL2-2-2‡	AF	p15.0-100.0+0	12	96.0	-69.9	1.0
	SL2-2-3‡	AF	p15.0-100.0+0	12	89.0	-79.1	1.4
	SL2-2-4‡	AF	p25.0-100.0+0	10	74.5	-74.7	2.4
	SL2-3-1	Th	p500.0-600.0+0	6	5.8	-45.1	2.9
	SL2-3-2	AF	p20.0-100.0+0	11	0.6	-44.4	1.9
	SL2-3-3	AF	p20.0-100.0+0	11	19.1	-48.1	2.9
	SL2-3-4	AF	p20.0-100.0+0	11	11.3	-46.4	2.2
	SL2-4-1	Th	p475.0-600.0+0	7	4.4	-19.8	4.4
	SL2-4-2	AF	p15.0-100.0+0	12	7.6	-22.8	1.5
	SL2-4-3‡	AF	p15.0-100.0+0	12	7.5	-19.4	2.1
	SL2-4-4	AF	p20.0-100.0+0	11	7.8	-22.7	1.5
	SL2-5-1	Th	p500.0-600.0+0	6	12.4	-43.5	5.4
	SL2-5-2	AF	p15.0-100.0+0	12	9.8	-39.5	1.0
	SL2-5-3	AF	p20.0-100.0+0	11	8.0	-40.3	4.4
	SL2-5-4	AF	p15.0-100.0+0	11	5.1	-37.1	1.4
	SL2-6-1	Th	p500.0-625.0+0	7	357.2	-37.9	6.9
	SL2-6-2	AF	p30.0-100.0+0	9	349.0	-40.5	2.3
	SL2-6-3	AF	p20.0-100.0+0	11	342.9	-37.5	1.3
	SL2-6-4	AF	p20.0-100.0+0	10	352.9	-39.7	2.3

<sup>‡:</sup> outlier removed from final analysis (further details may be found in Section 3, this Supplementary Information). The sampling code, e.g. "SL-A-B-C" is as follows: "SL", locality; "A", site, "B" fragment; "C", specimen.

**Table S8.** Archeomagnetic directional path divided into 5 arc segments, separated by cusps.

Arc distance (°)	Age difference (yr)	Rate (deg/yr)†	Localities Involved
$15.0 \pm 4.9$	$135 \pm 27$	$0.111 \pm 0.043$	Buhwa to RME 2
$19.1 \pm 4.7$	$215 \pm 27$	$0.089 \pm 0.025$	RME 2 to RME 1
$25.1 \pm 5.8$	$450 \pm 35$	$0.056 \pm 0.014$	RME 1 to AD300
$15.8 \pm 4.8$	$141 \pm 55$	$0.112 \pm 0.055$	AD300 to Icon
$23.0 \pm 4.0$	$180 \pm 63$	$0.128 \pm 0.050$	Icon to Kolope

 $<sup>\</sup>dagger~1\sigma$  uncertainty quoted.

# 3. Supporting Information Figures

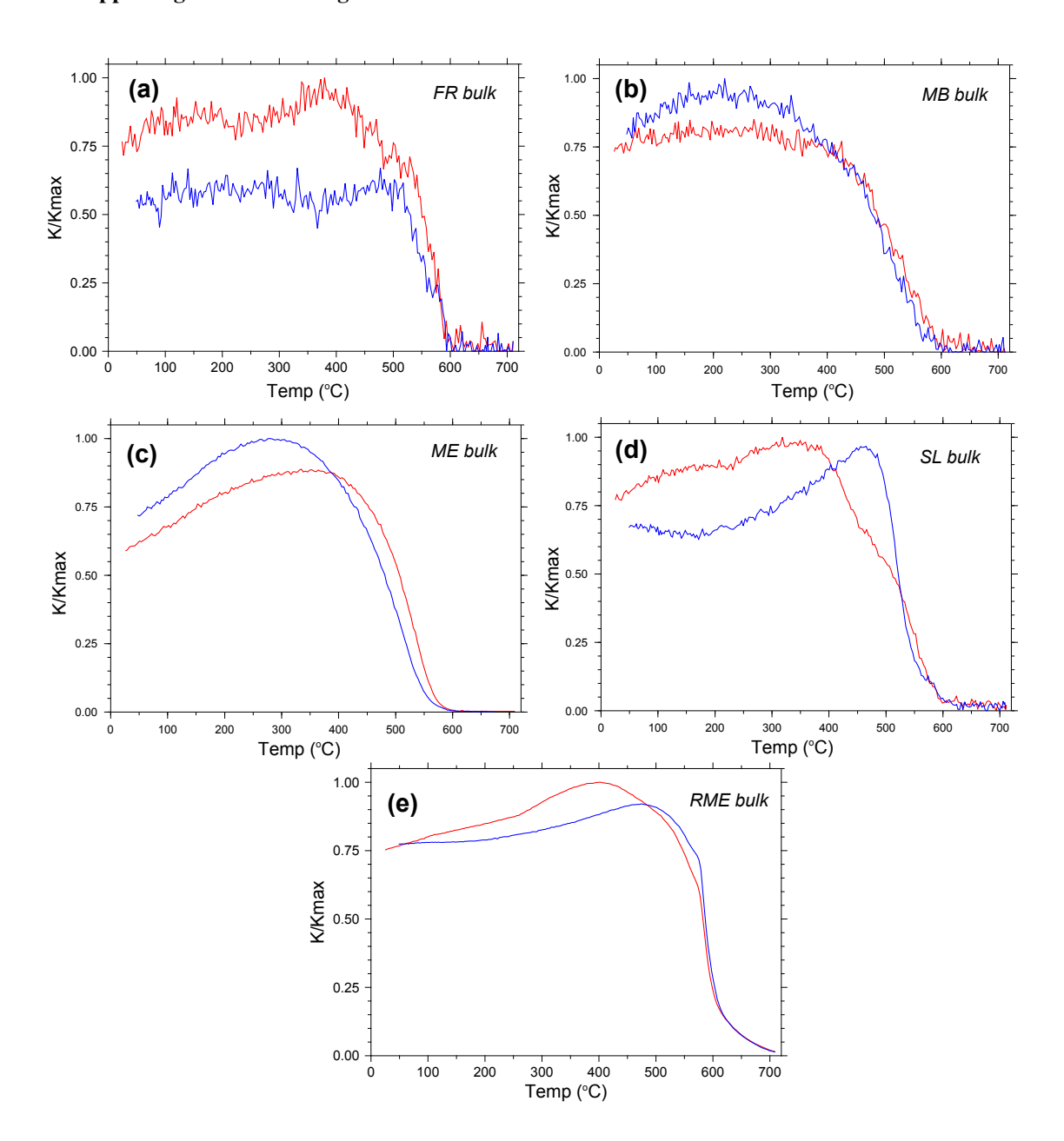


**Figure S2.** Low-field bulk magnetic susceptibility versus temperature for representative fragments. All magnetic susceptibility measurements were done in air with the Agico KLY-4S CS3 at the University of Rochester.

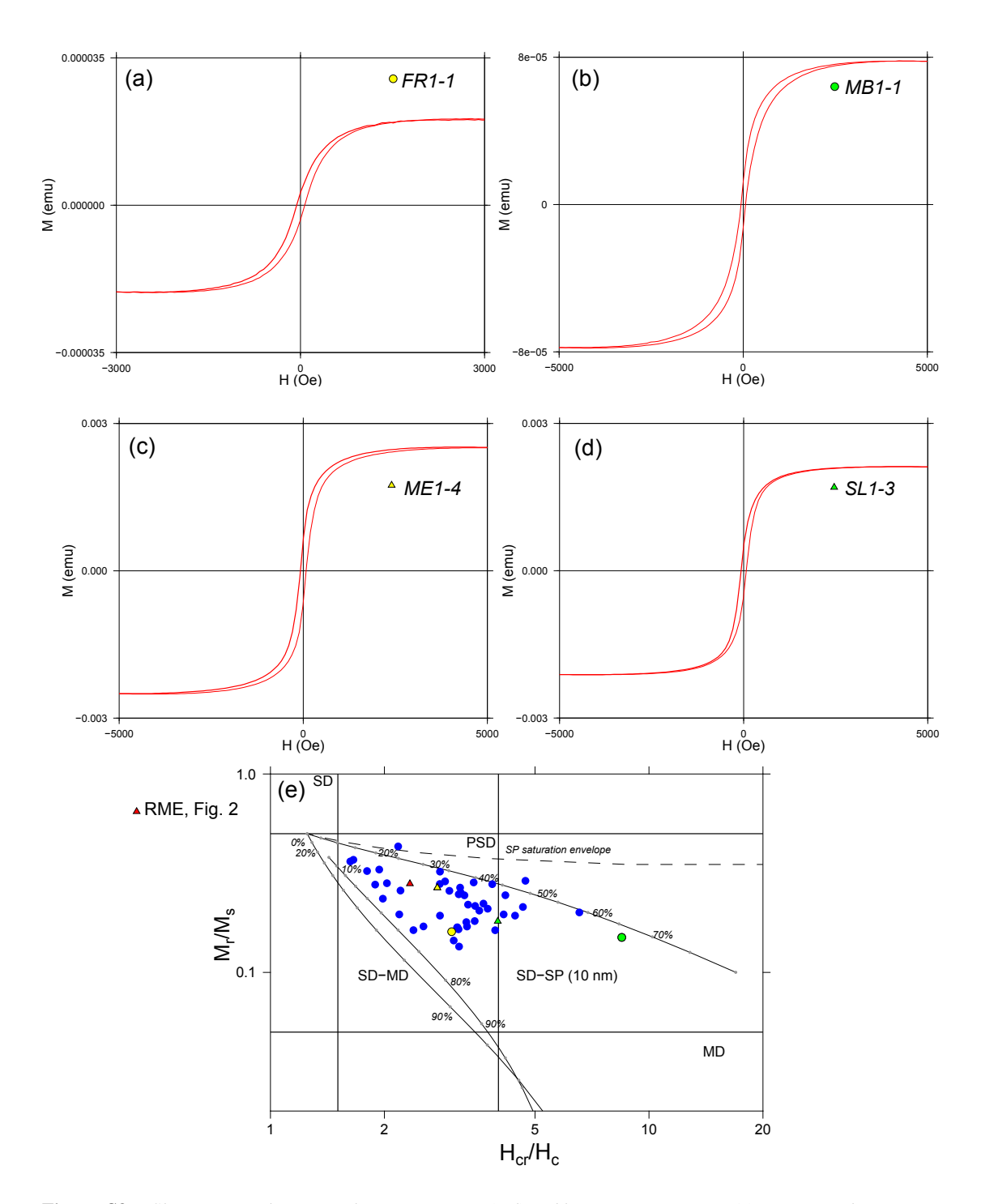


**Figure S3.** Slope corrected magnetic hysteresis curves (a-d) and hysteresis parameters (e) summarized on a Day plot (Day et al., 1977). Shown are reference single domain (SD) and multidomain (MD) mixing curves of Dunlop (2002). Other abbreviations: PSD, pseudo-single domain;  $M_r$ , saturation remanence;  $M_s$ , saturation magnetization;  $H_c$ , coercivity;  $H_{cr}$ , coercivity of remanence.

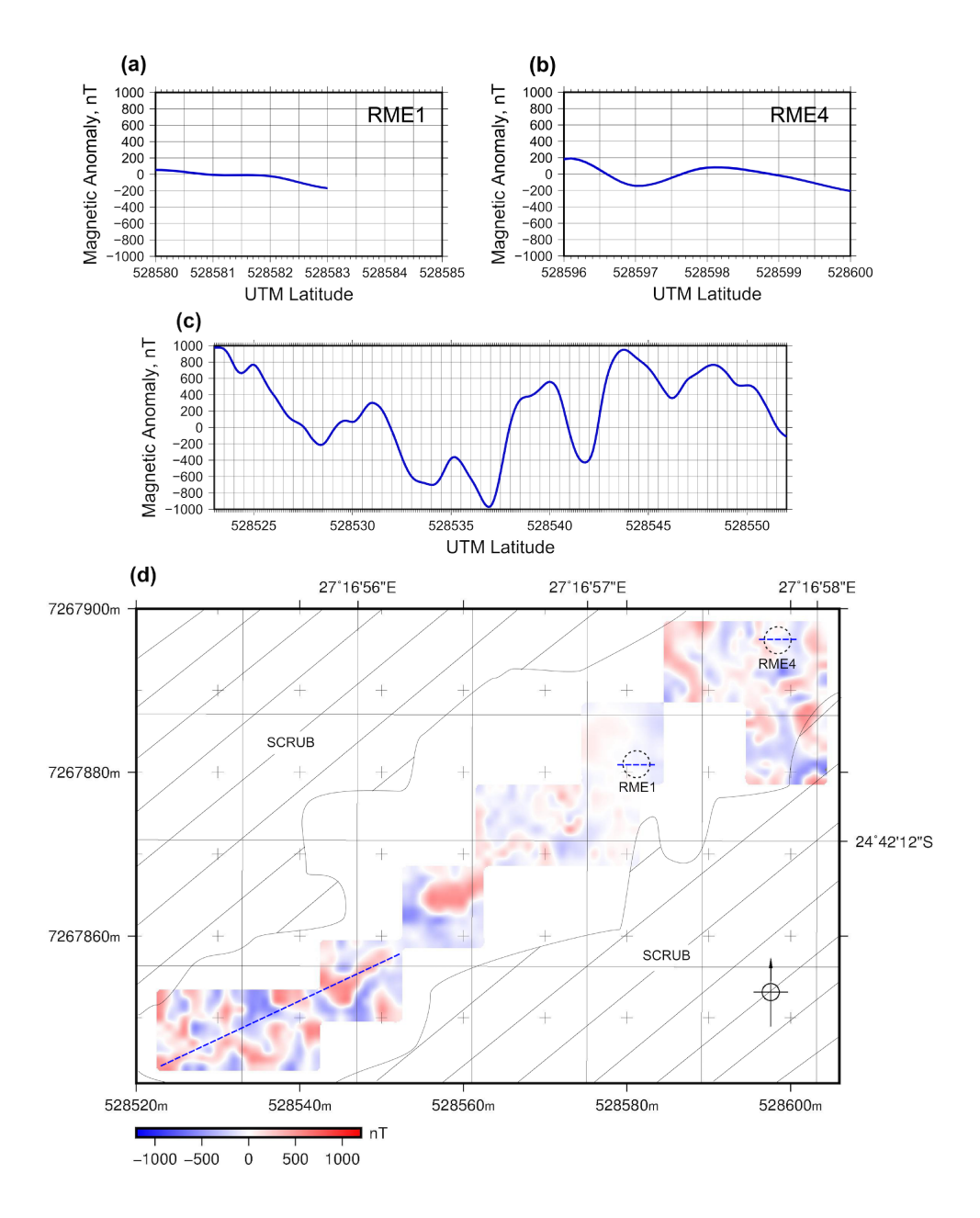


**Figure S4.** Field survey conducted for Rhino Mine (RME) localities. Magnetic anomaly maps, plotted in (d), were obtained using a Grad601 high-resolution fluxgate gradiometer (Bartington Instruments). (a) and (b show transects of field values through sites RME1 and RME4, which are indicated on (d) by dashed black lines. (c) shows transect of field values through lower left portion of map, indicated by dashed blue line.

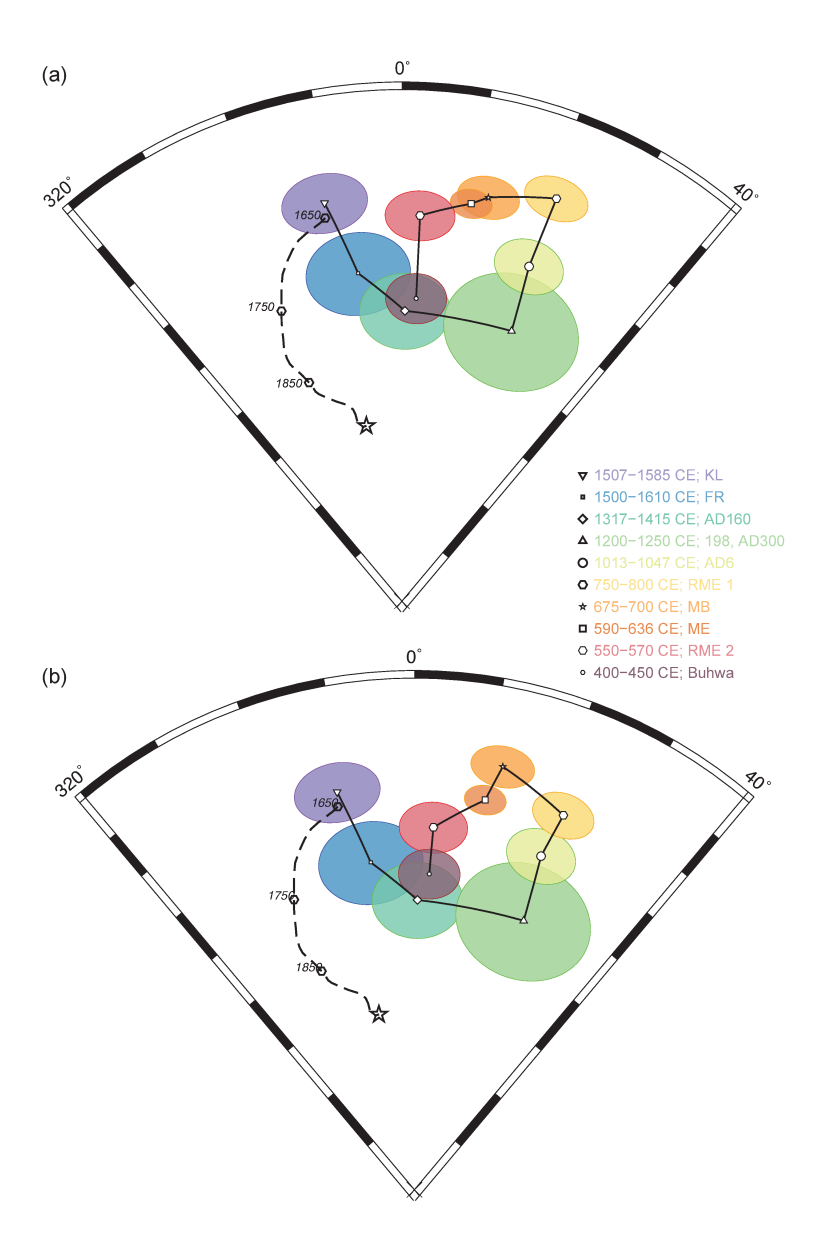


**Figure S5.** (a) stereonet of archaeomagnetic directional data from southern Africa after reduction to the geographic coordinates of Mapungubwe (22.212  $^{o}$  S, 29.387  $^{o}$  E). (b) stereonet of archaeomagnetic directional data before reduction procedure. Dashed black line shows field evolution from 1650 CE to the present according to the CALS3k.4 model.

#### 4. Outlier and exclusion procedure

We reject outlier directions which display angular distances more than  $3\times\alpha_{95}$  from the Fisher mean direction of each locality. First, the  $\alpha_{95}$  and Fisher mean is calculated including all specimen directions for each locality (see example in Fig. S6 below). Directions which are more than  $3\times\alpha_{95}$  are identified as outliers. This level is chosen as a balance between the sensitivity required to pick up data points which are visually identified as outliers and unnecessary loss of data, which may cause errors in estimation of Fisher means, as well as erroneously small  $\alpha_{95}$  values. After exclusion of outlier(s) the locality Fisher mean and  $\alpha_{95}$  is then recomputed, which taken as the final value.

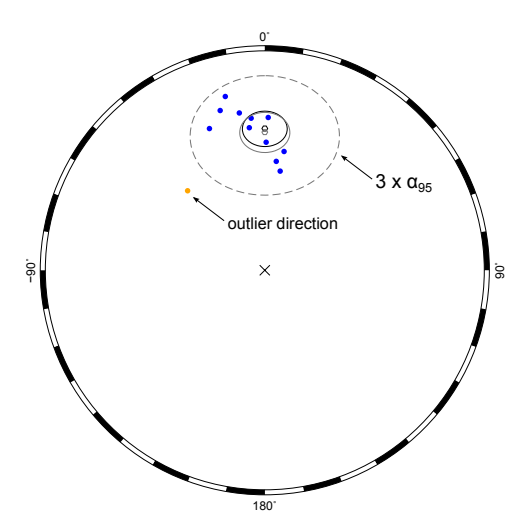


**Figure S6.** Illustration of outlier procedure for locality FR. Dashed grey confidence ellipse represents  $3 \times \alpha_{95}$  of original calculation including outlier. The Fisher mean is shown as a grey hexagon. Outlier is indicated in orange. Final  $\alpha_{95}$  and Fisher mean is shown as solid black confidence ellipse and hexagon.

We excluded between 0 (RME2) and 6 (ME) specimens per locality. There are several reasons that a direction may be identified as an outlier. In seven cases, one specimen from a fragment is rejected while others are retained, suggesting rock magnetic heterogeneity at the specimen level. In some instances, e.g. SL1, the procedure allows us to exclude an entire site. While directions from this site are still in the correct hemisphere, we suspect that fragments from this site were significantly disturbed either by weathering or vegetation growth, evident from site photos. It should also be noted that fragments from this particular grain bin exhibited poor thermal stability in susceptibility experiments, showing variable magnetic stability and probable maghemite conversion. This behavior might also explain poor coherence at the site level. Other examples, but at fragment level, is RME4, where both AF and thermal demagnetization directions from fragment RME4-8 are identified as outliers, and the entire fragment is excluded from the locality-level Fisher mean. Likewise, the entire SL2-2 fragment is excluded by our procedure. Both cases are most likely due to disturbance of fragments in the field. In these cases, the numerical procedure reliably identifies fragments and specimens which are known to be problematic by independent evidence (i.e. rock magnetic experiments or geological/archaeological information). Outliers from other sites are mostly directions obtained by AF demagnetization, and are excluded at the specimen level and not at the site/fragment level, most likely reflecting the aforementioned heterogeneity at the specimen level.

# 5. Model Comparisons

The principal feature that is defined in the data– but seen in variable degrees in model predictions – is a loop in the directional path. To further illustrate this, we show the direction defined between data of successive ages (Figure S7). In this format, the loop in the data is seen as a change from  $360^o$  (425-560 CE) to approximately  $49^o$  at 613-713 CE and back to  $262^o$  at 1225-1366 CE. AFM (Licht et al. 2013), ARCH3k\_1MAST (Korte et al. 2009) and SHA\_DIF\_14K (Pavón-Carrasco et al. 2014) show similar progressions but with age offsets. However, CALS3k.4 (Korte and Constable, 2011) misses the loop, whereas PFM9k (Nilsson et al. 2014) has, arguably, only a minor part of a loop.

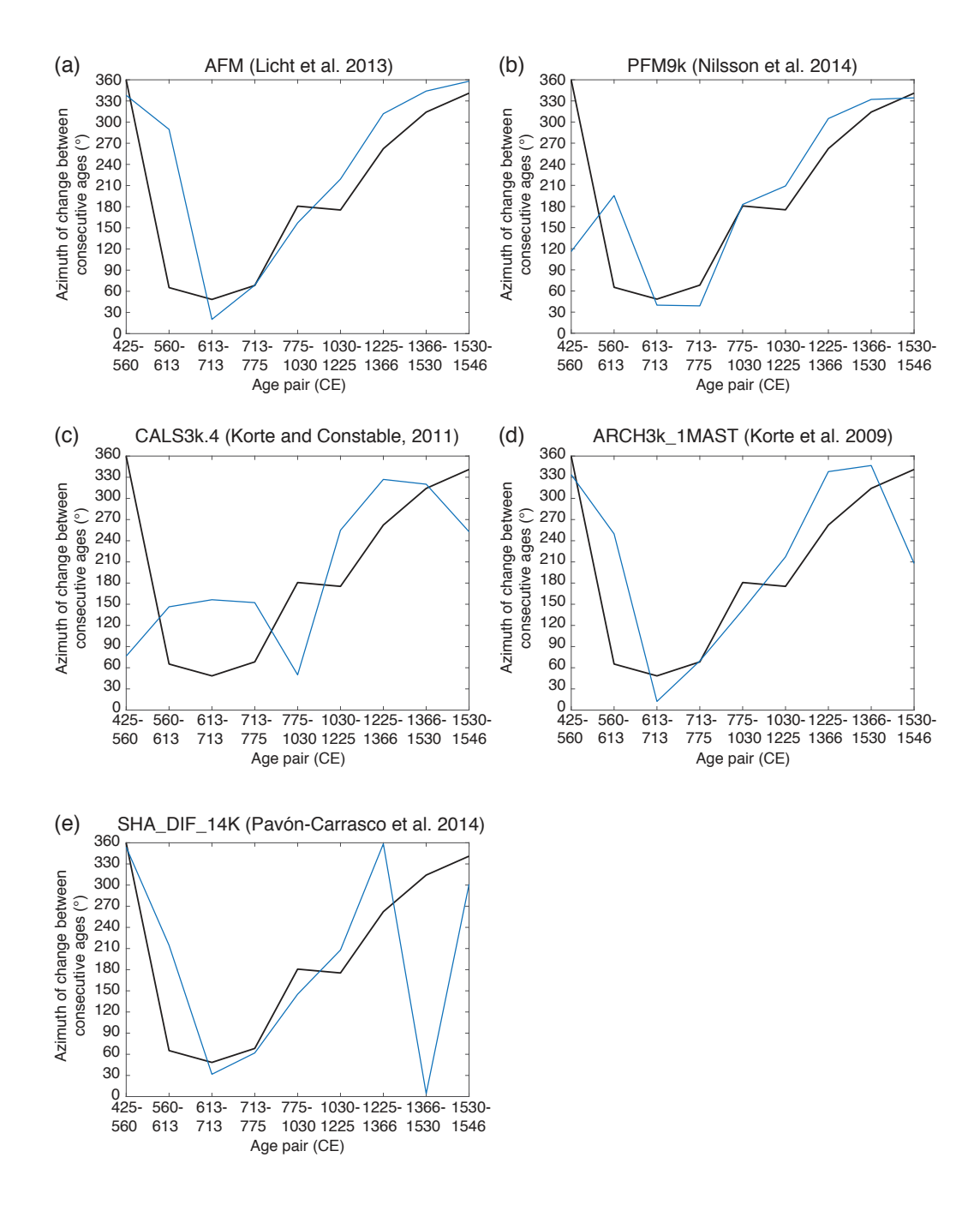


**Figure S7.** Comparison of the change in azimuthal direction between consecutive age-direction pairs Southern Africa paleomagnetic and archeomagnetic data of this study, combined with the data of Neukirch et al. (2012) and Tarduno et al. (2015), to the predicted geomagnetic field of five published field models. Paleomagnetic/archeomagnetic and field model predicted directions are reduced to a common site location (Mapungubwe: 22.212 °S, 29.387 °E). (a) black line: paleomagnetic/archeomagnetic; blue line: predicted geomagnetic field directions using the A\_FM model (Licht et al., 2013) for corresponding ages. (b) PFM9k geomagnetic field model of Nilsson et al. (2014). (c) CALS3k.4 (Korte and Constable, 2011). (d) ARCH3k.1(MAST) (Korte et al., 2009). (e) SHA\_DIF\_14K (Pavón–Carrasco et al., 2014).

#### 6. Archaeological localities and dating

**Buhwa** (2030CB19) was an early agricultural village located (20°36'03.9" S, 30°17'02.4" E) at the western base of Mount Buhwa, a large ironstone massif in central Zimbabwe (Huffman, 1978). The ceramic assemblage belongs to the Silver Leaves facies dated elsewhere to 280–450 CE (Huffman 2007: 123-125). Multiple grain bins were probably intentionally burnt as a ritual of cleansing during a severe drought that dated to between 400 and 450 CE (Huffman, 2009).

The Rhino Mine site (2427CB18) was also an early agricultural village located (24°4'11" S, 27°16'56" E) south of Thabazimbi in South Africa. The ceramic assemblage is dominated by the Happy Rest facies that dates to between 500 and 750 CE (Huffman, 2007: 219-221). Charcoal from a midden at the Rhino site has been radiocarbon dated to BP  $1550 \pm 80$  (Pta-9546) which calibrates (SHCal13) to 476-636 CE. The most probable span is 515-636 CE. Multiple grainbins were most likely burnt during a severe drought between 550 and 570 CE (Huffman, 2009). Our archaeomagnetic directions define two distinct phases (hence for consistency we identify two different localities "Rhino Mine I" and "Rhino Mine II"), the first associated with the RME1 and RME4 sites, and the second associated with RME2. On the basis of our stereonet evolution (Figure 4, main text), we suggest that the latter grain bin probably dates to this earlier phase between 550 and 570 CE, while RME1 and RME4 grain bins date to a later period between the  $7^{th}$  and  $8^{th}$ centuries CE, given the large age range of the Happy Rest facies (500 to 750 CE). Many early village sites were multicomponent. Multiple occupations were not obvious at Rhino Mine because the top layers had been removed through mining activity. Our archaeomagnetic directions define another phase after the sixth century. A carbonized post from RME 4 has been preliminarily dated to the last half of the eighth century CE (S. Woodborne, iThemba LABS, pers comm. 2017). This correlates with a severe drought sometime between 750 and 800 CE.

**Manong East** was an iron smelting village located ( $22^{o}11'06''$  S,  $27^{o}27'08''$  E) in a narrow valley in the Tswapong Hills in southeast Botswana (Huffman et al., 2016; Main, 2002, 2008). This site has not been dated but the same Happy Rest pottery was found at Manong West in an adjacent valley. Charcoal from a midden there has been radiocarbon dated to BP 1520  $\pm$  40 (Pta-7311) (Huffman 2007: 219), calibrating to 550-636 CE. The most likely dating span is CE 590–636.

**Mabveni** (2030AD5) was an early agricultural village located ( $20^{o}19'40.5"$  S,  $30^{o}28'31.8"$  E) in the Chivi District of southern Zimbabwe (Robinson, 1961). The pottery assemblage belongs to the Gokomere facies dated elsewhere to between 550 and 750 CE (Huffman 2007: 138-141). Charcoal from a midden excavated by Robinson has been radiocarbon dated to BP 1380  $\pm 110$  (SR 79) and BP 1365  $\pm$  30 (Pta-2105). The best calibrated span for these two dates is 670–750 CE. Within this span, the most likely associated drought was between 675 and 700 CE (Huffman, 2009).

**Faure** (2229AD2) was the headquarters of a petty chief in the Limpopo Valley dating to the Khami phase (Huffman and du Piesanie 2011). The small capital includes a stonewalled palace and several vitrified cattle kraals (Huffman et al., 2013). Charcoal from an associated midden has been radiocarbon dated to BP 390  $\pm$  40 (Pta-7971), calibrating to between 1463 and 1623 CE. The most likely dating span is 1500–1610 CE. If the vitrified kraals date to a known drought, the burnings most likely date to 1530  $\pm$  10 (Huffman, 2009). The Faure chief's village was probably contemporaneous with the nearby Kolope site (2229AD4), reported earlier (Tarduno et al., 2015).

#### References

- Day, R., Fuller, M., and Schmidt, V.A. 1977. Hysteresis properties of titanomagnetites: Grain size and composition dependence. *Physics of the Earth and Planetary Interiors* 13, 260–267.
- Dunlop, D.J. 2002. Theory and application of the Day plot  $(M_{rs}/M_s \text{ versus } H_{cr}/H_c)$  1. Theoretical curves and tests using titanomagnetite data. *Journal of Geophysical Research* 107, EPM4-1–EPM4-22.
- Huffman, T.N. 1978. The Iron Age of the Buhwa District, Rhodesia. *Occasional Papers National Museums Rhodesia A* 4(3), 2–22.
- Huffman, T.N. 2007. A Handbook to the Iron Age: The Archaeology of Pre-Colonial Farming Societies in Southern Africa. *Pietermaritzburg: University of KwaZulu-Natal Press*, 540.
- Huffman, T.N. 2009. A cultural proxy for drought: ritual burning in the Iron Age of Southern Africa. *Journal of Archaeological Science* 36, 991-1005.
- Huffman T.N. and du Piesanie, J. 2011. Khami and the Venda in the Mapungubwe land-scape. *Journal of African Archaeology* 9 (2), 189-206.
- Huffman, T.N., Elburg, M. and Watkeys, M. 2013. Vitrified cattle dung in the Iron Age of Southern Africa. *Journal of Archaeological Science* 40, 3553-3560.
- Huffman, T.N. and Woodborne, S. 2016. Archaeology, baobabs and drought: cultural proxies and environmental data from the Mapungubwe landscape. *The Holocene* 26(3), 464-470.
- Huffman, T.N., Thebe, P.C., Watkeys, M.K. and Tarduno, J. 2016. Archaeo-metallurgy in the Tswapong Hills; a preliminary report on archaeological context. *Southern African Humanities* 28, 119-133.
- Main, M. 2002. Tswapong Hills, Report, Archaeological Surveys 1996 2002. On file, National Museums and Art Gallery, Gaborone.
- Main, M. 2008.Report on Tswapong Hills archaeological surveys 1996-2002. Botswana Notes and Records 40, 55-59.
- Neukirch, L. P., Tarduno, J. A., Huffman, T. N., Watkeys, M. K., Scribner, C. A. and Cottrell, R. D., 2012. An archeomagnetic analysis of burnt grain bin floors from ca. 1200 to 1250 AD Iron–Age South Africa. *Phys. Earth Planet. In.* 190, 71–79.
- Pavón–Carrasco, F. J., Osete, M. L., Torta, J. M. and De Santis, A., 2014. A geomagnetic field model for the Holocene based on archaeomagnetic and lava flow data. *Earth Planet. Sci. Int.* 388, 98–109, doi:10.1029j.epsl.2013.11.046.
- Robinson, K.R. 1961. An Early Iron Age site from the Chibi District, Southern Rhodesia. *South African Archaeological Bulletin* 16, 95-102.
- Tarduno J.A., Watkeys, M.K. and Huffman, T.N. et al. 2015. Antiquity of the South Atlantic Anomaly: Evidence for top-down control on the geodynamo. *Nature Communications* 6, 7865. DOI: 10.1038/ncomms8865.